Geophys. J. Int. (2008) **173,** 1064–1083 doi: 10.1111/j.1365-246X.2008.03761.x

A high-resolution model for Eurasia–North America plate kinematics since 20 Ma

S. Merkouriev[1] and C. DeMets[2]

[1] *SPbFIZMIRAN, Muchnoj per,* 2*, Box* 188*, St. Petersburg* 191023*, Russia*

[2] *Department of Geology and Geophysics, University of Wisconsin-Madison, Madison, WI* 53706*, USA. E-mail: chuck@geology.wisc.edu*

Accepted 2008 February 14. Received 2008 February 14; in original form 2007 October 5

SUMMARY

We derive the first chronologically detailed model of Eurasia–North America plate motion since 20 Ma from ship and airplane surveys of the well-expressed magnetic lineations along this slowly spreading plate boundary, including previously unavailable dense Russian magnetic data from the southern Reykjanes Ridge and northern Mid-Atlantic ridge near the Charlie Gibbs fracture zone. From more than 7000 crossings of 21 magnetic anomalies from Anomaly 1n (0.78 Ma) to Anomaly 6n (19.7 Ma), we estimate best-fitting finite rotations and realistic uncertainties. Linear regressions of total opening distances versus their reversal ages at different locations along the plate boundary show that reversal boundaries are shifted systematically outwards from the spreading axis with respect to their idealized locations, with the outward shift ranging from more than 5 km between Iceland and the Charlie Gibbs fracture zone to ∼2 km elsewhere. This outward displacement, which is a consequence of the finite zone of seafloor accretion, degrades estimates of the underlying plate motion and is thus removed for the ensuing kinematic analysis. The corrected plate motion rotations reveal surprising, previously unrecognized features in the relative motions of these two plates. Within the uncertainties, motion was steady from 20 to 8 Ma around a pole that was located ∼600 km north of the present pole, with seafloor spreading rates that changed by no more than 5 per cent (1 mm yr^{-1}) along the Reykjanes Ridge during this period. Seafloor spreading rates decreased abruptly by 20 ± 2 per cent at 7.5–6.5 Ma, coinciding with rapid southward migration of the pole of rotation and a 5°–10° counter-clockwise change in the plate slip direction. Eurasia–North America plate motion since 6.7 Ma has remained remarkably steady, with an apparently stationary axis of rotation and upper limit of ±2 per cent on any variations in the rate of angular rotation during this period. Based on the good agreement between seismotectonic constraints on present deformation in northeast Asia and directions of motion that are predicted by our 6.7 Ma to present pole, we hypothesize that motion has remained steady to the present and attempt to test this hypothesis with published GPS estimates for Eurasia–North America motion. We find, however, that GPS estimates that are tied to recent versions of the international geodetic reference frame and rely principally on station velocities from Europe give implausible estimates of recent motion, with the most recently published GPS model predicting convergence along the southern Gakkel Ridge and in the Laptev Sea, where seafloor spreading occurs. An alternative GPS estimate that is not tied to the international terrestrial reference frame and employs GPS station velocities from northeastern Asia is marginally consistent with our 6.7–0 Ma motion estimate.

Key words: Plate motions; Continental neotectonics; Arctic region; Europe.

1 INTRODUCTION

Motivated by a desire to better understand the plate tectonic evolution of the Arctic basin and gain insights into a broad range of problems related to present-day and Cenozoic-era deformation of Eurasia and its collision boundaries with Nubia, Arabia, India and Australia, numerous authors have used marine and airborne magnetic and bathymetric data from the Arctic and North Atlantic ocean basins to reconstruct the post-120 Ma history of Eurasia–North America plate motion (e.g. Pitman & Talwani 1972; Srivastava & Tapscott 1986; Rowley & Lottes 1988; Lawver *et al.* 1990; Gaina *et al.* 2002; Glebovsky *et al.* 2006). Estimates of motion during the

Neogene (23 Ma to the present) from these studies have focused principally on reconstructions of magnetic anomaly 2A (3 Ma), Anomaly 5 (11 Ma) and Anomaly 6 (19.7 Ma), each of which is clearly expressed in the North Atlantic and Arctic. These well determined rotations have significantly improved our understanding of deformation in northeast Asia during the Neogene (Cook *et al.* 1986; Gaina *et al.* 2002). However, the ∼8 Myr spacings between the reconstructions for Anomalies 2A, 5 and 6 are too large to determine with precision the timing of any changes in plate motion over the past 20 Ma and correlate such changes with on-land geological events or changes in motion along other plate boundaries.

In this study, we present the first chronologically detailed model of Eurasia–North America plate motion since 20 Ma, using marine magnetic data from parts of the plate boundary between the Azores triple junction (Fig. 1) and northern end of the Kolbeinsey ridge. Our work is motivated by three distinct lines of inquiry. The first is whether any changes in seafloor spreading between the Eurasian and North American plates is correlated in time with an abrupt change in India–Somalia plate motion that occurred at ∼10–9 Ma (Merkouriev & DeMets 2006). A temporal correlation between the motions of the Indian and Eurasian plates, which share a wide convergent boundary that includes the Himalayan mountain belt, would imply that plate driving stresses are transferred efficiently across this plate boundary and are thus capable of propagating outwards to induce changes elsewhere in the global plate circuit. Our second goal is to determine whether the Eurasia–North America pole may have changed location once or possibly twice over the past 10 Myr, as inferred by Cook *et al.* (1986) and Riegel *et al.* (1993) from their interpretation of seismologic and structural observations in northeastern Asia. Our third motivation is to provide an improved basis for interpreting Global Positioning System (GPS) estimates of Eurasia–North America motion within the context of a detailed geologic model for the relative motions of these two plates (e.g. Kogan *et al.* 2000; Paul *et al.* 2001; Calais *et al.* 2003; Steblov *et al.* 2003).

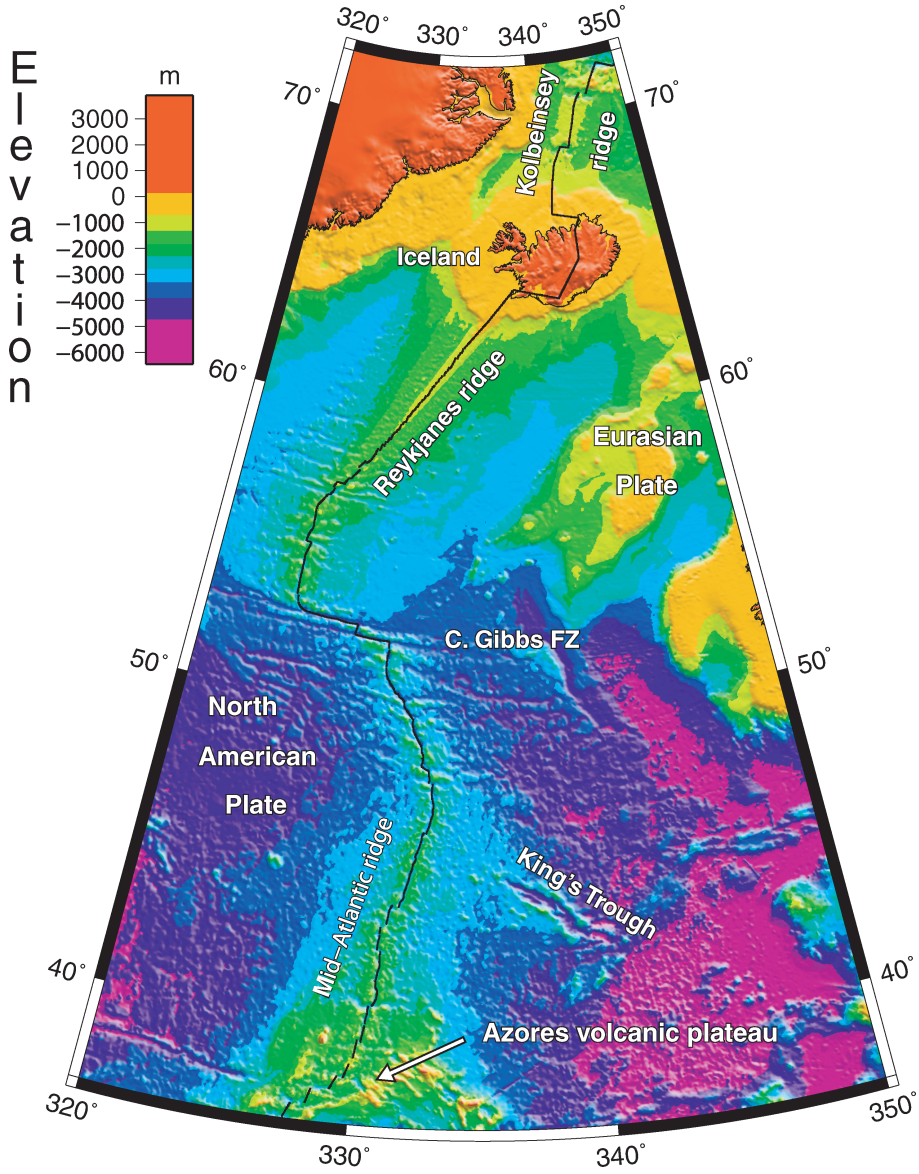

Figure 1. A—Locations of major features described in text overlaid on 2 min topography and bathymetry from Sandwell & Smith (1997). Abbreviations: C. Gibbs FZ – Charlie Gibbs fracture zone.

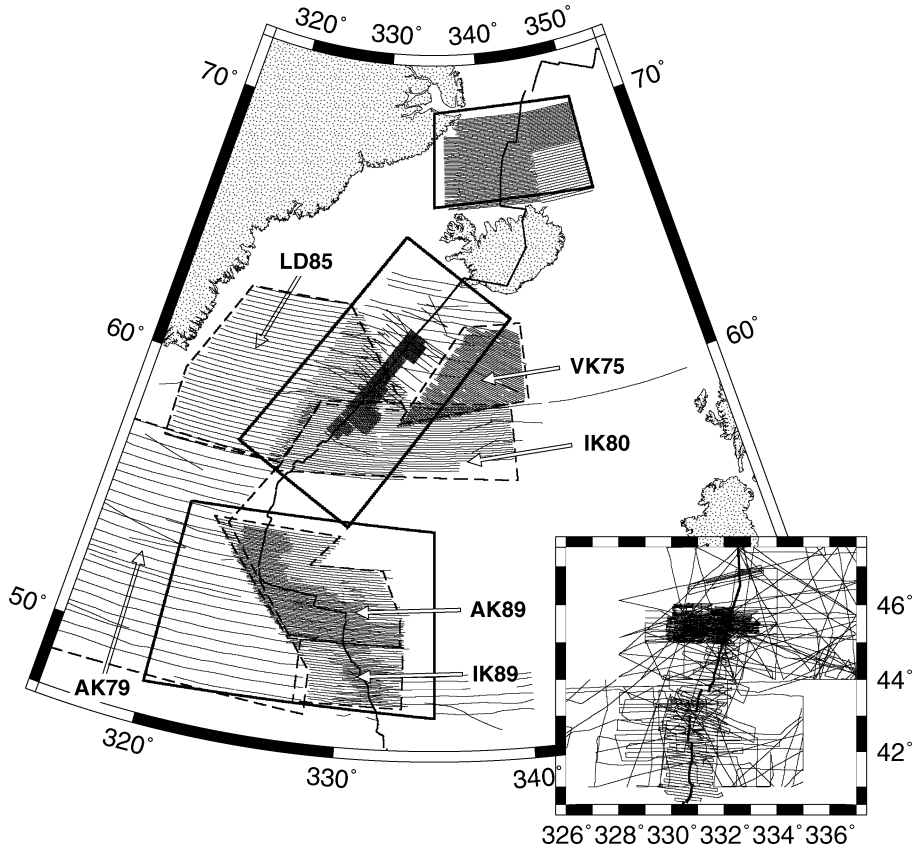

Figure 2. Tracks of shipboard and airborne magnetic anomalies employed in this study. Dashed rectangles outline limits of Russian surveys VK75, AK79, IK80, LD85, AK89 and IK89 used for the analysis. Inset shows ship and airplane tracks for magnetic anomalies north of the Azores triple junction. Magnetic anomalies in the areas designated with bold lines and within the inset map are shown in Figs S1–S3.

2 DATA: MAGNETIC ANOMALY CROSSINGS

The data used for our analysis span the southern half of the 8000-km-long series of Arctic and Atlantic basin seafloor spreading centres that accommodate motion between Eurasia and North America (Figs 1 and 2). The magnetic anomalies in much of this region are unusually clear and complete for slow seafloor spreading centres and are thus well suited for constructing a detailed plate motion model. The most comprehensive compilation of magnetic anomaly data in the Arctic and North Atlantic basins is that described by Verhoef *et al.* (1996), who incorporate millions of magnetic measurements from hundreds of cruises and airplane surveys between 1956 and 1992 into a magnetic anomaly grid with 5-km-cell spacing. We chose not to employ this grid for our analysis because its 5-km-cell spacing undersamples some of the shorter wavelength magnetic anomalies that we use in our analysis. We instead use original shipboard and airborne magnetic data (Fig. 2) from a variety of sources described below, including a significant amount of data that is not incorporated into the Verhoef *et al.* 5 km grid.

Russian shipboard magnetics that were gathered during cruises from 1975 to 1989 (VK75, IK80, LD85, AK79, AK89 and IK89) constitute our primary source of our data between 49°N and 64°N. Of these, only the data from cruises AK79, LD85 and VK75 are incorporated in the Arctic and North Atlantic digital magnetic database (Verhoef *et al.* 1996). The Russian data, which significantly improve coverage of areas of the southern Reykjanes ridge and northern Mid-Atlantic Ridge near the Charlie Gibbs fracture zone where few data are otherwise available, are complemented by dense track coverage of young magnetic anomalies along the Reykjanes Ridge from 59.5°N to 62.5°N (Searle *et al.* 1998) and additional ship tracks compiled from the U.S. National Geophysical Data Center (NGDC). The magnetic anomalies from all these sources (shown in the Supplementary Material available in the online version of the article, Figs S1 and S2B) reveal complete, relatively uninterrupted magnetic reversal sequences out to seafloor ages of at least 20 Ma in most areas between 51°N and Iceland. The superbly defined, highly lineated magnetic anomalies along the Reykjanes Ridge strongly constrain the history of Eurasia–North America motion along this part of the plate boundary and anchor our kinematic model.

Along the Kolbeinsey ridge north of Iceland, we use a dense aeromagnetic survey done in 1973 by the US Naval Oceanographic Office (Vogt *et al.* 1980). Consisting of dozens of closely spaced ridge-normal track lines (shown in Fig. S2A), the track lines reveal a clearly defined magnetic anomaly sequence from the present out to 20 Ma, interrupted only by a ridge axis re-organization at the time of Anomaly 3A (Appelgate 1997). Between the Azores triple junction and 48°N (Fig. S3), we extracted magnetic anomaly crossings from the dense TRIATNORD survey (Goslin *et al.* 1999; Gente *et al.* 2003), from surveys archived at the NGDC, and from two dense Canadian surveys of the ridge from 45°N to 46°N (Verhoef *et al.* 1996; S. Dehler 2000, personal communication). The track coverage of magnetic anomalies younger than 4n.1 (7.5 Ma) between the Azores triple junction and 48°N is superb and strongly constrains motion for these times. The coverage of the reversals

Table 1. Data and magnetic anomaly age summary.

Anomaly	Age (in Ma)	N_{anom}	m_{anom}
1no	0.781	602	54
2ny	1.778	632	33
2An.1y	2.581	683	38
2An.3o	3.596	562	41
3n.1y	4.187	404	33
3n.4o	5.235	396	28
3An.1y	6.033	394	30
3An.2o	6.733	307	28
4n.1y	7.528	374	33
4n.2o	8.108	353	23
4Ao	9.098	276	22
5n.1y	9.779	340	26
5n.2o	11.040	344	27
5An.2o	12.415	228	20
5ACy	13.734	144	16
5ADo	14.581	148	15
5Cn.1y	15.974	200	17
5Dy	17.235	153	15
5Ey	18.056	194	16
6ny	18.748	188	17
6no	19.722	230	19

Anomaly ages are from Lourens *et al.* (2004). Chron designators followed by a 'y' or 'o' respectively indicate the young or old edge of the chron. N_{anom} indicates the number of magnetic anomaly crossings that are used to constrain the finite rotation for a given anomaly. m_{anom} indicates the number of palaeospreading segments used to fit the reversal crossings for that time.

older than Anomaly 4n.1 is sparser, but is, nonetheless, sufficient to provide useful constraints on the reconstructions for times older than Anomaly 4n.1.

From these numerous data, we selected all crossings of 21 magnetic polarity reversals (Table 1), ranging in age from 0.781Ma (the old edge of Anomaly 1n) to 19.7 Ma (the old edge of Anomaly 6). The 21 correlation points coincide with either the young or old edge of a magnetic polarity interval (Fig. 3) and are assigned ages from the Lourens *et al.* (2004) astronomically-tuned geomagnetic reversal timescale. We use 7150 magnetic anomaly crossings (Fig. 4) for our kinematic analysis, ranging from as few as 144 to as many as 683 for the individual magnetic reversals (Table 1).

We did not use any crossings of oceanic fracture zones to constrain the Eurasia–North America finite rotations, primarily because the finite rotations for all but two times (Anomaly 1n and 2n) are already well constrained by the reconstructed magnetic lineations. For Anomalies 1n and 2n, we used two points located along the Charlie Gibbs transform fault to enforce a pole location that predicts small circle motion along the transform fault.

3 ANALYSIS TECHNIQUES

3.1 Estimation of finite rotations and uncertainties

Fitting criteria described by Hellinger (1979) are used to derive the rotations that best reconstruct the magnetic anomaly crossings of a given age from opposite sides of the seafloor spreading centre. For a palaeoplate boundary that can be divided into P distinct spreading segments (or fracture zones), the measure of misfit for each reconstructed spreading segment is determined by summing the weighted least-squares distances of all the anomaly crossings that are affiliated with the reconstructed segment from their best-fitting great circle segment. The overall measure of misfit for a trial rotation is the sum of the misfits for the P reconstructed segments. The best-fitting rotation is determined using a downhill simplex technique (Chang 1988), with modifications described below to correct for systematic shifts in anomaly locations due to the effect of outward displacement.

Following Royer & Chang (1991), we use $\hat{\kappa} = (N - m)/\chi^2$ as a measure of the dispersion of the observations with respect to

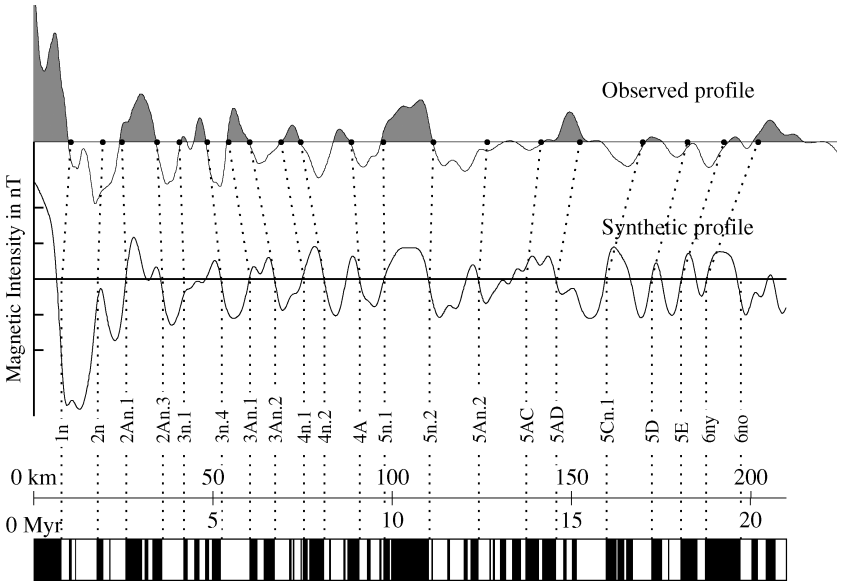

Figure 3. Correlation points for the 21 magnetic anomalies for which Eurasia–North America motion is modelled. The observed magnetic profile, from cruise BAP75 from the National Geophysical Data Center archives, extends eastwards from the axis of the Reykjanes Ridge in a nearly flow-line parallel direction. The one-sided synthetic magnetic profile was created using a full spreading rate of 20 km Myr^{-1}, a 500-metre-wide reversal transition zone and ambient and palaeomagnetic inclinations and declinations appropriate for the study region. The magnetic block model and 21 correlation points (dotted lines) used for this study appear below the synthetic magnetic anomaly profile.

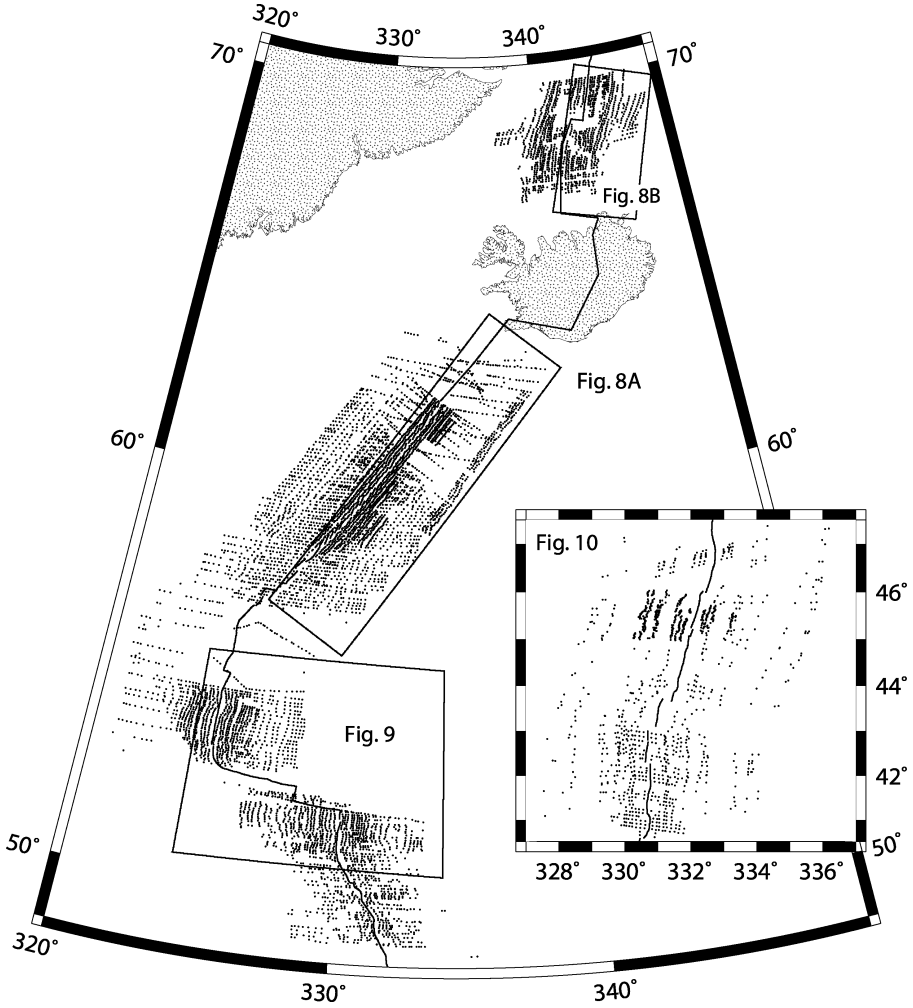

Figure 4. Magnetic anomaly crossings for the 21 reversals identified in Table 1 and Fig. 3. Detailed views of the anomaly crossings within the designated areas are shown by the anomaly reconstructions in Figs 8–10. Figs S1–S3 show the magnetic anomalies that are the basis for these anomaly correlations.

the predictions of our best-fitting rotations, where N is the number of anomaly crossings that are used to estimate the finite rotation, m is the number of parameters that are used to fit the data and χ^2 is the weighted least-squares fit of the rotation that best fits the data. The number of model parameters m is equal to $3 + 2 \times P$, where P is the total number of great circles that are used to fit the reconstructed data. Values of $\hat{\kappa} \simeq 1$ indicate that the data uncertainties are approximately correct, whereas values of $\hat{\kappa}$ significantly greater or less than 1 indicate that the uncertainties are respectively overestimated or underestimated by a factor of $\sqrt{\hat{\kappa}}$.

Merkouriev & DeMets (2006) demonstrate that uncertainties in finite rotations are caused by a combination of random errors in anomaly crossing locations and two sources of systematic error. One source of systematic error, referred to hereafter as outward displacement, is attributable to the finite-width zone across which new seafloor accretes and records magnetic polarity transitions (Sempere *et al.* 1987). It shifts all anomaly crossings outward from their idealized locations by distances that range 1–6 km along the mid-ocean ridge system (DeMets & Wilson 2008). A second source of systematic error, referred to hereafter as segment-specific systematic error, contributes an additional ±1 km of systematic uncertainty to the locations of all anomaly crossings from a given spreading segment and may represent variations in the local magnitude of outward displacement with respect to a boundary-wide average value.

Rotation covariances that do not account for the segment-specific systematic errors may understate the true rotation uncertainties by a factor or two or more (Merkouriev & DeMets 2006). We therefore incorporate these errors into our finite rotation uncertainties using a segment-based bootstrapping technique that samples a wider range of possible segment weightings than would otherwise be sampled by a single inversion of the anomaly crossings for a given time. A description of this technique is given by Merkouriev & DeMets (2006) (their section 4.4) and is not repeated here.

The best-fitting rotations described later in the analysis are the average of 1000 rotations derived from inversions of bootstrapped data for each of the 21 magnetic anomalies considered in this study. The rotation covariances are derived from the 3×3 orientation matrix (Fisher *et al.* 1993) for the 1000 bootstrapped rotations and constitute more realistic estimates of the likely uncertainties in the rotation parameters for a given time.

We derive stage rotations from the finite rotations to describe motion during intervals of 1–3 Myr or longer. The uncertainties in the stage rotations are propagated rigorously from the finite rotation covariances. Seafloor spreading rates that we estimate from the stage rotations require reversal age estimates, which can introduce

errors into the estimated stage rates. For magnetic reversals whose ages are astronomically calibrated, errors in their estimated ages are unlikely to exceed ±5000–10 000 yr (Lourens *et al.* 2004). The implied standard error in a stage spreading rate that averages motion over 1.5 Myr, the approximate length of the shortest averaging interval that we use, is only 0.6 per cent of the stage rate or about ±0.1 mm yr^{-1} for the 15–20 mm yr^{-1} full spreading rates that are typical of Eurasia–North America motion. Such errors are a factor of 2–10 smaller than the uncertainties propagated from the rotation covariances and thus do not represent an important limiting factor in our analysis. In addition, the bias in our estimates of finite rotations from outward displacement does not significantly affect the stage rotations because this bias is common to all of the finite rotations and is thus completely cancelled upon differencing those rotations to estimate stage rotations.

3.2 Correction for outward displacement

Outward displacement of geomagnetic reversal boundaries modifies the expected sinusoidal variation of seafloor opening distances with angular distance from the pole of opening and must thus be estimated and removed to determine the true pole of opening and opening angle for a plate pair. For example, outward displacement varies from 2 to 6 km in our study area (Section 4.1) and constitutes a substantial fraction of the 10–15 km of seafloor spreading that has occurred during Anomaly 1n. We correct for the effect of outward displacement on the location of the pole and its opening angle in two stages. Our procedure for estimating best-fitting rotations (Section 3.1) includes small-angle, location-dependent corrections to the total opening angle to compensate for differences in the magnitude of outward displacement along the plate boundary. Without such corrections, anomaly crossings from areas of the plate boundary with anomalously wide or anomalously narrow outward displacement would be, respectively, under- or overrotated by the best-fitting rotation.

We further corrected each best-fitting rotation by adding to it a small-angle counter-rotation that removes the equivalent of 2 km of opening everywhere along the plate boundary, equal to our best estimate of the uniform value for outward displacement. Our two-stage correction for the effect of outward displacement thus first compensates for differential outward displacement during the fitting procedure and then corrects for the effect of the remaining uniform-magnitude outward displacement. Further details, including the relative effects of these corrections on the estimated

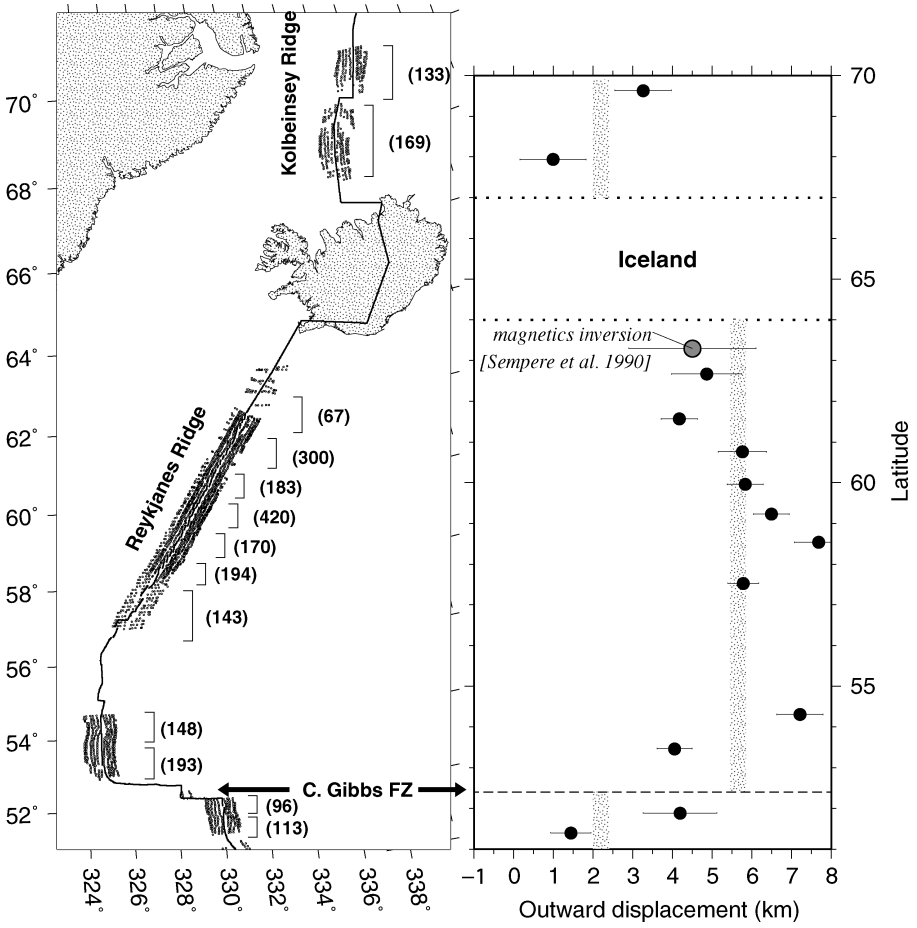

Figure 5. *Y*-axis intercepts (right-hand side panel) from linear regressions of opening distance time-series for Anomalies 1n, 2n, 2An.1, 2An.3 and 3n.1, constituting kinematic estimates of outward displacement (see the text). Brackets in left-hand side panel indicate geographic limits of the anomaly crossings, which are used to derive the optimal opening angles and hence opening distances from which the estimates of outward displacement (filled circles in the right-hand side panel) and their 1σ uncertainties are derived. The numerals within the parentheses indicate the number of anomaly crossings that are used to derive the sequence of best opening angles from each geographical subgroup. Vertical shaded lines in the right-hand side panel show our best estimates of outward displacement for ridge segments between Iceland and the Charlie Gibbs fracture zone and for the remaining ridge segments. The scatter of the individual *Y*-axis intercepts (circle) with respect to the best estimates is not statistically significant (see the text).

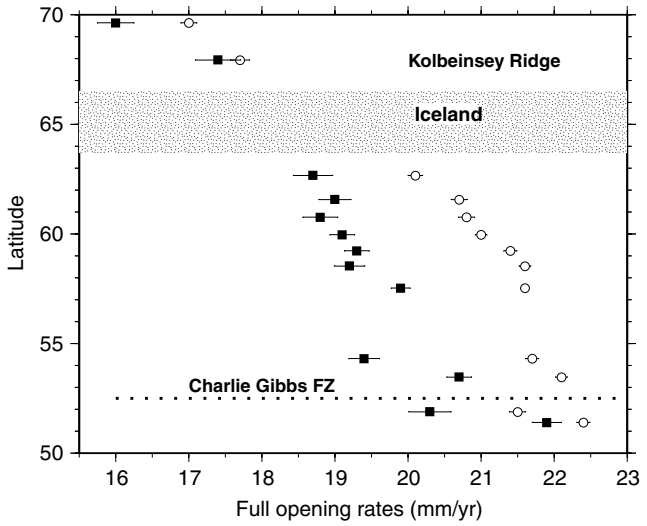

Figure 6. Seafloor spreading rates in the study area with (solid squares) and without (open circles) a correction for outward displacement. Individual opening rates are determined from a linear regression of the sequence of total opening distances for Anomalies 1n, 2n, 2An.1, 2An.3 and 3n.1 for the 13 anomaly subgroups shown in Fig. 5.

rotations, are given in Section 4.5. Hereafter, we refer to the rotations that are corrected only for variable-magnitude outward displacement as the best-fitting reconstruction rotations. These rotations reconstruct anomaly crossings from one side of a spreading centre onto their counterparts across the ridge in a best-fitting least-squares sense. We refer to the rotations that are also corrected for the effect of uniform-magnitude outward displacement as plate motion rotations because they describe plate motion after removing most or all of the bias from outward displacement.

4 RESULTS

4.1 Evidence and corrections for outward displacement

Along a seafloor spreading centre where opening rates have remained constant for the past few million years, as appears to be true for the Eurasia–North America plate boundary, outward displacement of magnetic reversals with respect to their idealized locations will be manifested as positive-valued, distance-axis intercepts for regressions of seafloor opening distances as a function of their reversal ages. We tested systematically for the existence and magnitude of outward displacement within our study area as follows: We first divided the anomaly crossings into 13 geographically distinct spreading corridors (Fig. 5a). From the crossings of Anomalies 1n, 2n, 2An.1, 2An.3 and 3n.1 within each corridor, we then derived a best-fitting opening angle for each anomaly assuming a fixed rotation pole throughout. We then estimated a total opening distance at the geographic midpoint of each spreading corridor, yielding 13 linearly independent sequences of seafloor opening distances as a function of reversal age.

Linear regressions of each of the 13 distance versus reversal-age sequences yield 13 positive-valued distance-axis intercepts

Table 2. Eurasia–North America finite rotations from data bootstrapping.

Chron	DOF	Lat.	Long.	Ω	Covariances					
		°N	°E	(degrees)	a	b	c	d	e	f
1n	493	66.89	137.20	−0.196	14.1	−7.4	24.7	4.2	−13.0	48.2
2n	565	62.20	138.79	−0.385	8.7	−4.5	16.5	3.5	−7.8	34.5
2An.1	607	63.63	137.44	−0.559	4.9	.6	5.1	5.1	−7.7	21.1
2An.3	480	61.84	139.00	−0.761	18.9	2.2	17.4	10.8	−10.7	35.9
3n.1	338	63.83	135.81	−0.892	30.4	1.3	25.0	10.8	−17.1	56.4
3n.4	340	61.10	137.88	−1.090	25.8	−1.0	32.4	20.1	−28.4	85.5
3An.1	334	63.29	135.33	−1.256	12.7	−1.7	17.9	13.0	−21.3	57.8
3An.2	251	65.73	134.86	−1.461	51.7	−11.5	77.0	33.4	−67.5	207.5
4n.1	308	63.21	137.38	−1.593	29.5	−5.1	43.3	27.1	−49.2	138.5
4n.2	307	64.43	137.29	−1.783	48.5	−4.6	59.3	38.2	−70.4	193.2
4A	232	64.86	135.65	−2.053	75.8	−14.6	100.2	82.9	−160.5	394.3
5n.1	288	66.10	137.62	−2.268	264.6	42.7	200.5	112.0	−126.9	421.6
5n.2	290	67.75	133.17	−2.622	81.4	−12.5	100.1	53.5	−107.0	298.0
5An.2	188	67.19	133.86	−2.988	929.2	19.0	835.4	169.7	−260.9	1241.4
5AC	112	67.39	132.58	−3.346	3255.6	−756.4	4366.0	254.0	−1141.9	6084.2
5AD	118	69.50	127.69	−3.685	11925.3	−2535.8	15099.3	838.7	−3712.3	20022.7
5Cn.1	166	67.97	133.21	−4.017	1368.7	−120.9	1473.9	198.3	−431.3	2097.9
5D	123	68.85	129.75	−4.386	1003.8	−129.5	1269.6	75.9	−240.0	1716.5
5E	162	70.16	129.10	−4.708	1238.3	−326.9	1783.3	116.3	−518.1	2656.0
6ny	154	72.12	126.70	−5.048	3408.3	−185.2	4169.4	475.6	−717.2	5665.5
6no	192	68.62	131.76	−5.029	616.3	−74.2	717.0	50.8	−156.3	964.2

DOF is degrees of freedom, which equals the total anomaly and fracture zone crossings for a given chron minus twice the sum of the total number of segments and the number of rotation parameters (3). Rotations reconstruct Eurasia plate relative to North America plate and incorporate the correction for variable-magnitude outward displacement that is described in the text. Rotations that are further corrected for the effect of uniform outward displacement are given in Table 3. Covariances are Cartesian and have units of 10^{-8} radians^2. Covariances are attached to Eurasia plate. Elements a, d and f are the variances of the (0°N, 0°E), (0°N, 90°E) and 90°N components of the rotation, respectively. The covariance matrices are reconstructed as follows.

$$\begin{pmatrix} a & b & c \\ b & d & e \\ c & e & f \end{pmatrix}$$

(Fig. 5b). The intercept values range from 1–2 km near the Charlie Gibbs fracture zone and along the Kolbeinsey ridge to 7.5 km along the Reykjanes ridge. Using identical techniques, DeMets & Wilson (2008) report outward displacement of 1–2 km for the ridge segments north of the Azores triple junction. Outward displacement is thus 1–2 km for most spreading corridors in our study area, but is larger between the Charlie Gibbs fracture zone and Iceland.

Fig. 6 shows average seafloor opening rates since Anomaly 3n.1 (4.19 Ma) in the 13 spreading corridors with and without any correction for outward displacement. The uncorrected opening rates decrease rapidly between 70°N and 58.5°N and then exhibit little or no change south of 58.5°N, contrary to the expected sinusoidal change. In contrast, the corrected rates (e.g. the slopes derived from linear regressions of the 13 age-distance sequences) increase systematically from the northern end of the Kolbeinsey Ridge to the Charlie Gibbs fracture zone, as expected.

Sempere *et al.* (1990) estimate the width of magnetic polarity transition zones at the northern end of the Reykjanes Ridge from inversions for seafloor magnetization of shallow-water magnetic profiles near Iceland. These inversions yield magnetic polarity transition zone widths of 2–8.4 km, with an average of 4.5 ± 1.6 km. These agree remarkably well with our independent, kinematically-derived estimates (Fig. 5b) and argue against the possibility that an acceleration of Eurasia–North America seafloor spreading rates over the past 780 000 yr is responsible for the uniformly positive distance-axis intercepts that we obtain from our age-distance regressions.

We tested for the simplest description of outward displacement along the plate boundary by gathering the young anomaly crossings into successively larger geographic groupings and repeating the age-distance analysis described above. The data are fit poorly if we estimate only one value for outward displacement for the entire plate boundary, but are well fit by a model in which outward displacement has a uniform value of 5.5 km between the Charlie Gibbs fracture zone and Iceland and 2 km everywhere else along the plate boundary. All rotations described below are corrected using these two values for outward displacement.

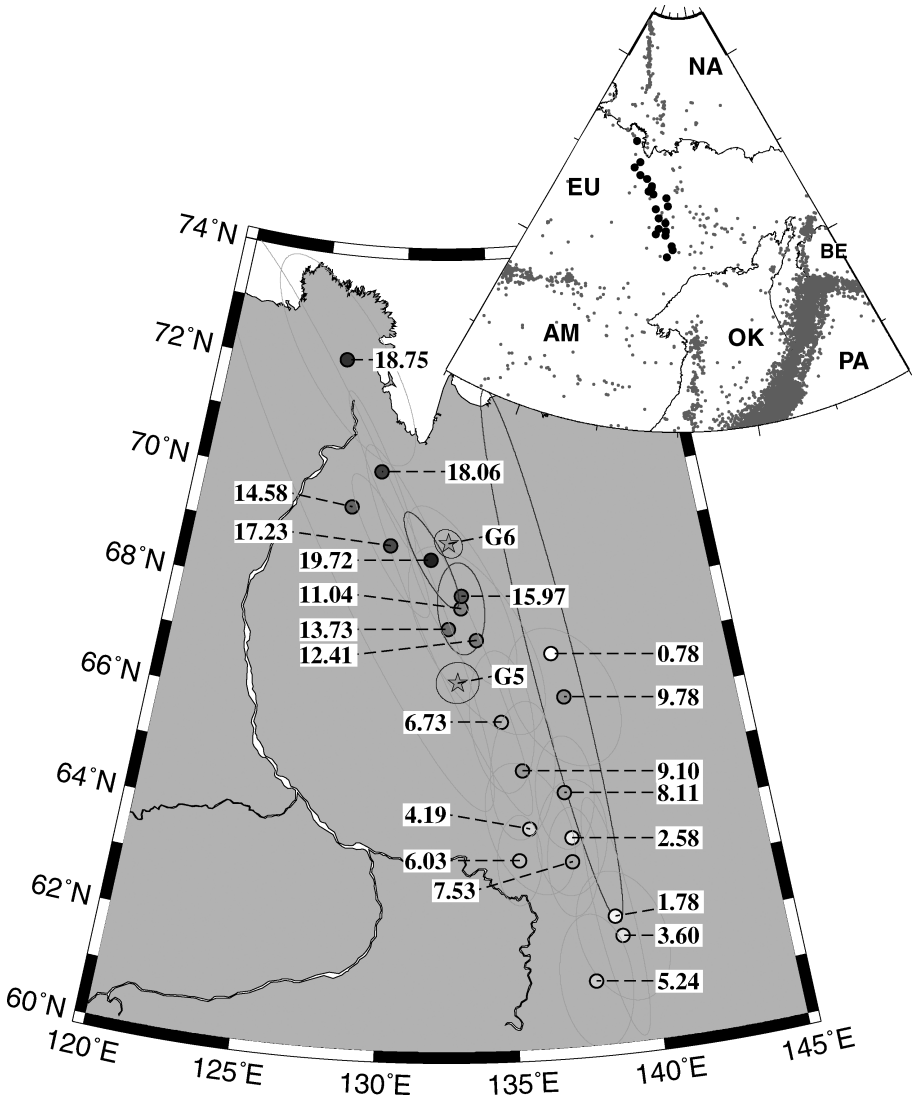

Figure 7. Eurasia–North America best-fitting reconstruction poles (Table 2) and their ages in millions of years. Ellipses show 2-D, 1σ confidence regions determined from bootstrapping procedure that is described in the text. For clarity, only the confidence regions for Anomalies 1n (0.78 Ma), 5n.2 (11.04 Ma) and 6no (19.72 Ma) are shown. Stars labelled 'G5' and 'G6' designate locations of Anomaly 5n.2 and 6no finite opening poles from Gaina *et al.* (2002). Inset shows pole locations (filled circles) and 1963–2007 shallow earthquakes (shaded circles). Plate abbreviations are AM – Amurian; BE – Bering; EU – Eurasian; OK – Okhotsk; NA – North American; PA – Pacific.

4.2 Best-fitting rotations, poles and lineation reconstructions

Using procedures described in Section 3.1, we estimated a best-fitting pole and opening angle for each of the 21 sets of reversal crossings (Table 2), including use of a small-angle correction during the fitting procedure to compensate for wider outward displacement between Iceland and the Charlie Gibbs fracture zone. The best-fitting reconstruction poles are shown in Fig. 7 and the best-fitting reconstructions are shown in Figs 8–10.

The finite opening poles (Fig. 7) are located between 61°N and 72°N and exhibit some evidence for time-dependent pole migration. Beginning with Anomaly 6no, the pole locations for progressively younger magnetic reversals migrate southwards, with poles for the oldest reversals (Anomalies 5n.2–6no) located from 66°N to 72°N and poles for all younger reversals except Anomaly 1n located from 62°N to 66°N (Fig. 7). The poorly constrained pole location for Anomaly 1n reflects the more poorly determined opening gradient for this anomaly relative to the underlying data uncertainties and is consistent within its uncertainties with the more southerly pole locations for the other young magnetic reversals. Further discussion of the apparent pole migration is given in Section 4.5.2

Our reconstructions of the Reykjanes Ridge magnetic lineations afford a clear view of the changes in its axial geometry since 20 Ma (Fig. 8a). A major change in the configuration of the ridge geometry is evident at 59°N for Anomaly 6no (19.7 Ma), with the palaeo-axis north of 59°N exhibiting oblique seafloor spreading similar to that observed in the present and the palaeo-axis south of 59°N exhibiting segmented, ridge-normal seafloor spreading. By the time of Anomaly 3n.1 (4.19 Ma), the transition point between the two differing axial geometries had migrated southward by 400 km to 57.2°N, 327.4°E, at the southern limit of the dense magnetic data that we use for this study. We are presently investigating,

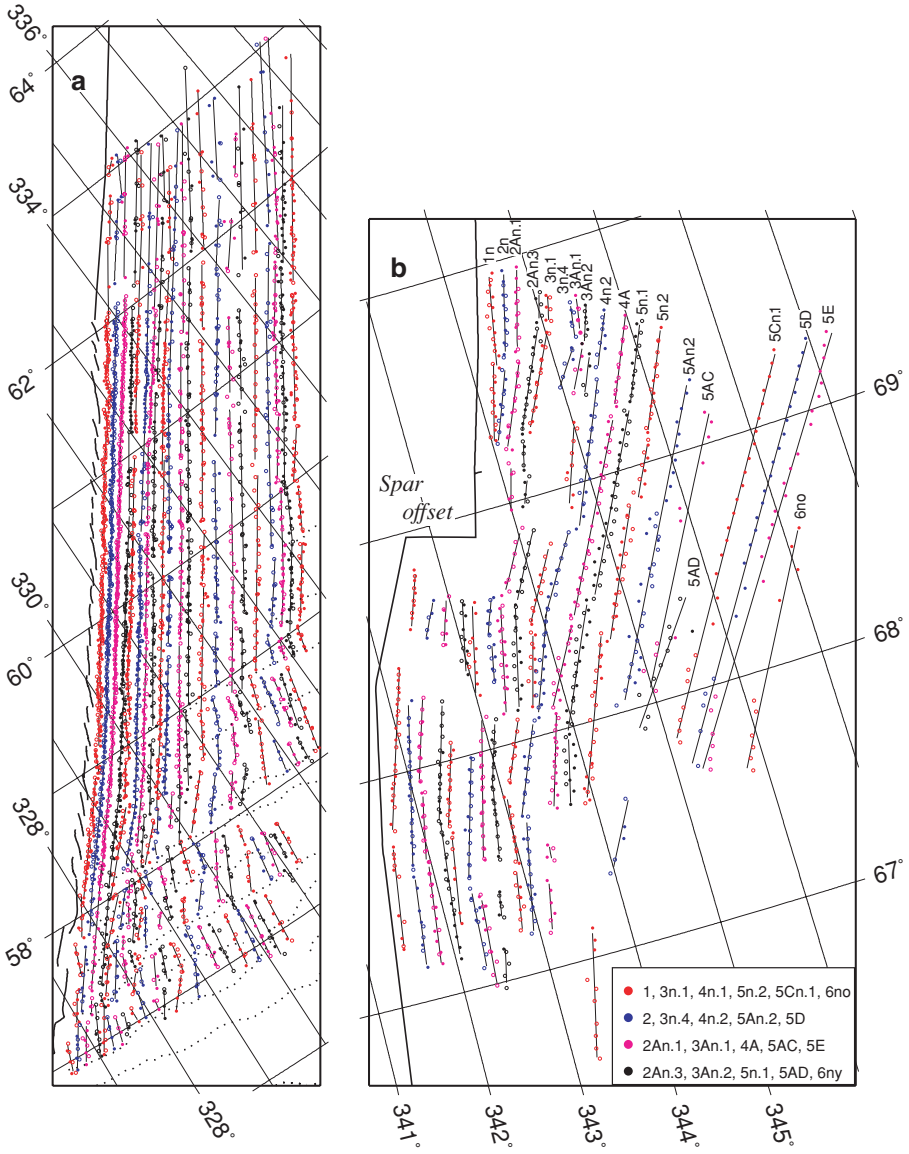

Figure 8. Reykjanes (a) and Kolbeinsey Ridge (b) anomaly crossings from the North American plate (open circles) reconstructed onto Eurasia plate anomaly crossings (filled circles) using best-fitting rotations in Table 2. Dashed lines show present locations of discontinuities in the marine gravity field (courtesy of A. Briais 2006, personal communication).

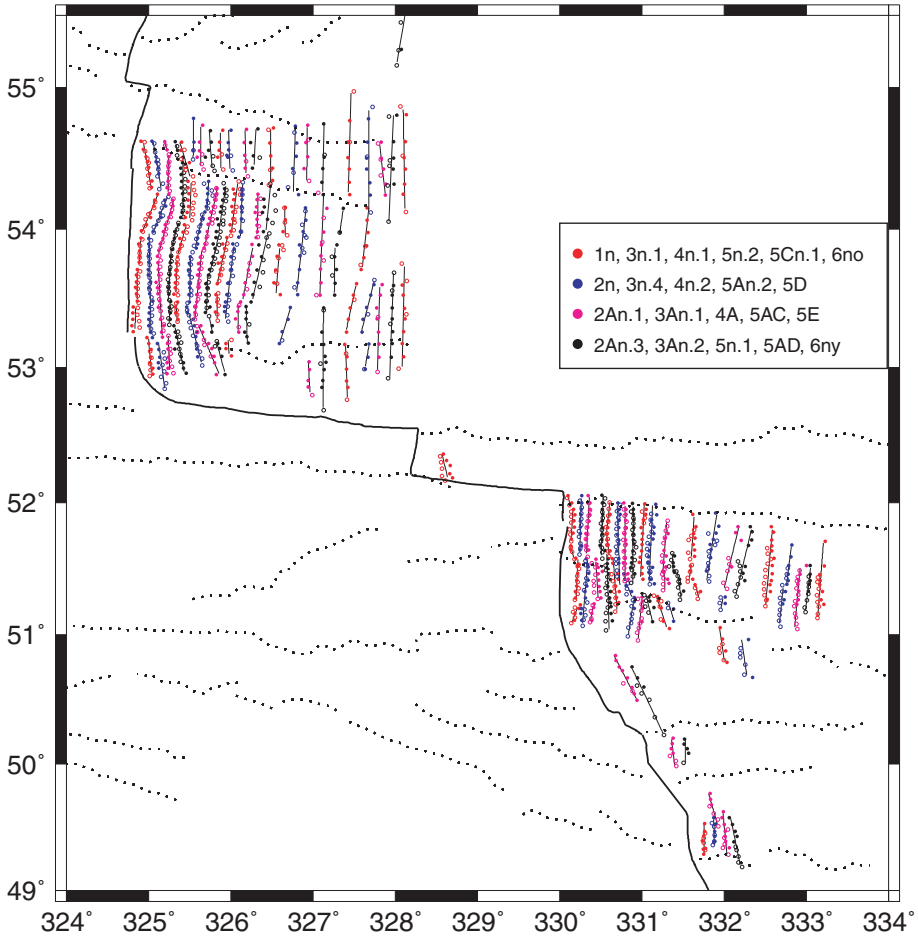

Figure 9. Magnetic anomaly crossings from North American plate (open circles) reconstructed on to Eurasia plate anomaly crossings (filled circles) using best-fitting rotations in Table 2. Dashed lines show present locations of discontinuities in the marine gravity field (courtesy of A. Briais 2006, personal communication).

in more detail, the spatial and temporal history of this transition in the mode of seafloor accretion and do not further discuss this topic below.

Our reconstructions of the Kolbeinsey ridge magnetic lineations (Fig. 8b) indicate that the ridge axis was relatively continuous at the time of Anomaly 4A, but began rotating counter-clockwise by Anomaly 4n.2 and rapidly developed a major offset (the Spar offset) during Anomaly 3A (6.6–5.9 Ma). Our results confirm those of Appelgate (1997), who employs the same aeromagnetic data to identify the reorganization of the ridge geometry during Anomaly 3A.

Our reconstructions of the well expressed magnetic lineations immediately north and south of the Charlie Gibbs fracture zone (Fig. 9) indicate that the palaeo-axial geometry there has remained relatively constant for the past 20 Ma. Similarly, the more sparsely surveyed magnetic lineations north of the Azores triple junction (Fig. 10) show no obvious evidence of a widespread axial reorganization since 20 Ma.

4.3 Data fits

We determined the magnitude of random and segment-specific errors in our data from a two stage error analysis. Random errors in the anomaly crossing locations were determined from separate inversions of the anomaly crossings for each palaeospreading segment to find their dispersion with respect to their respective best-fitting great circle segment. For the 7150 anomaly crossings and 551 palaeospreading segments that are used to fit them, 68.3 per cent of the residual distances are smaller than 1.1 km after adjusting for the number of parameters that are used to fit the observations. Reflecting this dispersion, the uncertainties that we assigned to individual anomaly crossings are slightly larger than ± 1.0 km, with some variation in the uncertainties that we assigned to individual anomaly crossings depending on the type of navigation used for a given cruise or flight. All of the data uncertainties are adjusted in the final stage of the analysis so that $\hat{\kappa}$ for each best-fitting rotation is close to its expected value of 1.

We estimated segment-specific errors by determining the degree of under- or over-rotation of anomaly crossings for each palaeospreading segment when reconstructed using the best-fitting rotations from Table 2. On average, the segment-specific misfits are $\sim$1 km larger than should occur for data with underlying random errors of 1.1 km. This corroborates results reported by Merkouriev & DeMets (2006) for segment-specific errors of $\sim$1 km along for the India–Somalia plate boundary. The segment-specific biases are incorporated into the rotation uncertainties, as described in Section 3.1.

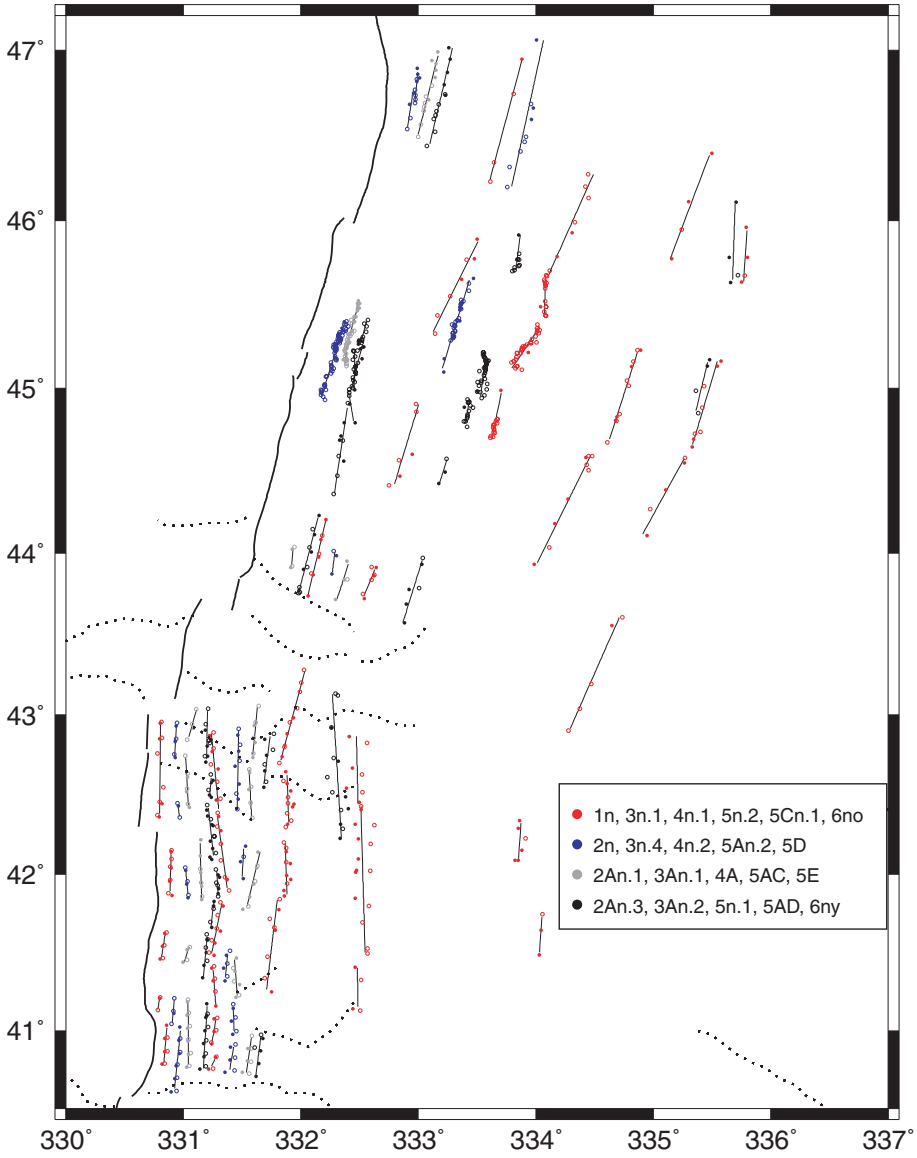

Figure 10. Magnetic anomaly crossings from North American plate (open circles) reconstructed onto Eurasia plate anomaly crossings (filled circles) using best-fitting rotations in Table 2. Dashed lines show present locations of discontinuities in the marine gravity field (courtesy of A. Briais 2006, personal communication).

4.4 Comparison with Gaina *et al.* (2002) results

We compared our rotations and data fits for Anomaly 5n.2 and 6no with those reported by Gaina *et al.* (2002), who estimate best-fitting finite rotations for both of these reversals using data extracted from the Arctic and North Atlantic magnetic anomaly grid (Macnab *et al.* 1995; Verhoef *et al.* 1996) and the marine gravity grid of Sandwell & Smith (1997). The total opening distances that are predicted for Anomaly 5n.2 by our best-fitting rotation and that of Gaina *et al.* (2002) differ by only 1 per cent at a central location along the Reykjanes ridge. Similarly, the two models predict total opening distances for Anomaly 6no that differ by only 1 per cent. Given that the poles for both of these anomalies from the two studies also agree within their 2-D 95 per cent confidence limits (Fig. 7), we conclude that the two models predict motions that are the same within uncertainties.

We also compared the dispersions of the crossings of Anomaly 5n.2 and 6no, which are used in the two studies to assess the internal consistencies of the data used in both studies. Relative to our best-fitting reconstructions (Figs 8–10), our crossings of Anomaly 5n.2 and 6no have a dispersion of 1.1 km. The dispersion of the anomaly crossings used by Gaina *et al.* (2002) to derive their best-fitting reconstructions is 3.3 km. We suspect that the factor-of-three difference in the dispersions for the two studies is caused by the coarser 5 km resolution of the magnetic anomaly grid that Gaina *et al.* employ for their analysis, although local misidentifications of Anomaly 5n.2 or 6no might also contribute to their larger misfits.

4.5 Eurasia–North America plate motion since 20 Ma

To model the evolution of Eurasia–North America plate rates and slip directions since 20 Ma, we applied a small clockwise rotation

Table 3. Eurasia–North America plate motion rotations.

Chron	Lat. °N	Long. °E	Ω (degrees)
1n	70.21	135.71	−0.182
2n	63.65	138.38	−0.369
2An.1	64.65	137.07	−0.544
2An.3	62.56	138.82	−0.746
3n.1	64.47	135.52	−0.877
3n.4	61.59	137.73	−1.074
3An.1	63.73	135.12	−1.241
3An.2	66.14	134.65	−1.446
4n.1	63.56	137.27	−1.578
4n.2	64.75	137.18	−1.768
4A	65.14	135.52	−2.038
5n.1	66.37	137.54	−2.254
5n.2	67.99	133.03	−2.608
5An.2	67.39	133.75	−2.974
5AC	67.57	132.47	−3.331
5AD	69.67	127.52	−3.671
5Cn.1	68.13	133.12	−4.003
5D	69.00	129.63	−4.372
5E	70.30	128.98	−4.694
6ny	72.25	126.56	−5.035
6no	68.74	131.68	−5.015

Rotations from Table 2 perturbed by a clockwise rotation of 0.018° about a pole located at Ω = 30.6°N, 143.2°E to correct for the influence of 2 km of outward displacement along the plate boundary. These rotations are the best estimates of Eurasia–North America motion from the present back to the specified magnetic anomaly. Rotation covariances are identical to those in Table 2.

of 0.018° about a pole located at Ω = 30.6°N, 143.2°E to each of the best-fitting reconstruction rotations from Table 2 to correct for the effect of uniform-magnitude outward displacement on the rotation estimates. This small-angle rotation predicts 2 km of closing everywhere between the Azores triple junction and northern end of the Kolbeinsey Ridge and thus effectively corrects the best-fitting reconstruction rotations for 2 km of outward displacement. The resulting Eurasia–North American plate rotations (Table 3) constitute our best estimates of the relative plate motion.

The small-angle correction described above yields plate motion rotations that are closer to the plate boundary than their corresponding reconstruction rotations and also reduces by approximately 2 km the predicted opening distances everywhere along the plate boundary. The correction has the largest effect on the reconstruction rotations with the smallest opening angles. For example, the Anomaly 1n rotation is shifted 3.3 angular degrees closer to the plate boundary and predicts opening rates that are 10–15 per cent (2 mm yr^{-1}) slower after being corrected by the small-angle rotation. In contrast, the rotation for Anomaly 5n.2, which has a much larger opening angle, moves only 0.25 angular degrees closer to the plate boundary and predicts long-term seafloor spreading rates that are only 1 per cent slower, too small to change any of the major conclusions reached in this study.

4.5.1 Orthogonal rotation component time-series

Employing techniques pioneered by Stock & Molnar (1983) and Wilson (1993), we assessed the steadiness of plate motion since 20 Ma by decomposing each of the plate motion rotations into a component that describes the gradient in opening distances along the plate boundary (Ω_{skew} in Fig. 11) and a second, orthogonal component that describes uniform opening along the plate boundary (Ω_{mag} in Fig. 11). During periods of constant plate motion, each of these orthogonal rotation angles increases linearly with time. Their dimensionless ratio therefore also remains constant during periods of steady motion, thereby providing a robust proxy for periods of constant plate motion and the timing of any changes in motion.

The time sequence of orthogonal rotation angles shown in Fig. 11 exhibits only one clear change since 20 Ma, namely at the time of Anomalies 4n.1 to 3An.2 (7.5–6.7 Ma). The well constrained orthogonal components are consistent with constant motion from the present back to at least Anomaly 3An.2 (6.7 Ma) and possibly Anomaly 4n.1 (7.5 Ma) (see lower panel of Fig. 11). Similarly, the orthogonal components for reversals older than Anomaly 4n.1 are also consistent with constant motion from 20 to 7.5 Ma within their larger uncertainties. The plate motion rotations are thus consistent with a two-stage motion model since 20 Ma, consisting of steady motion from 20 to 7.5 Ma, an apparently abrupt change in motion at ∼7.5 Ma and steady motion from ∼7 Ma to the present.

Given that this is the first evidence for a change in Eurasia–North America motion at ∼7 Ma, we next examine, in more detail, the evidence for a two-stage model of Eurasia–North America motion since 20 Ma.

4.5.2 Smoothed and stage pole locations

Fig. 12 shows a smoothed sequence of plate motion poles determined by averaging the plate motion rotations from Table 3 over several-million-years-long time windows over the past 20 Myr. Relative to the noisier sequence of best-fitting reconstruction poles (Fig. 7), the smoothed poles more clearly migrate southward through time. To determine when the pole changed its location, we calculated stage rotations from the plate motion rotations in Table 3. The stage poles (not shown) for times between the present and 6.7 Ma (Anomaly 3An.2) are consistently clustered near 63°N–64°N, 137°E and support a model in which the pole location has been stationary since 6.7 Ma. In contrast, the stage poles for times older than 7.5 Ma (Anomaly 4n.1) are located near 70°N, 127°E and within their larger uncertainties suggest that the pole was fixed from 20 to 7.5 Ma. The stage poles are therefore consistent with a change in the pole location at ∼7 Ma.

4.5.3 Stage spreading rates

From the stage rotations described above, we estimated stage spreading rates along a flow line centred on the Reykjanes Ridge, where the dense and unambiguous magnetic data impose the strongest and most reliable constraints on the spreading history (Fig. 13a). The rate of seafloor spreading from 20 to 8 Ma averaged 23.5 ± 1 mm yr^{-1} and, within the uncertainties, either remained steady during this entire period or accelerated modestly. Seafloor spreading rates between 7.5 and 6.7 Ma slowed abruptly by 15–20 per cent to 19.5 ± 0.5 mm yr^{-1}, coinciding with the change in motion indicated by the orthogonal rotation components (Fig. 11). The opening rate since 7.5 Ma has remained steady within a range of ±0.5 mm yr^{-1}.

Although the change in stage spreading rates at 7.5–6.7 Ma is a robust outcome of our analysis, some of the variations in the stage rates results from either errors in the reversal age estimates that we use or possibly systematic mispicking of the tie points that

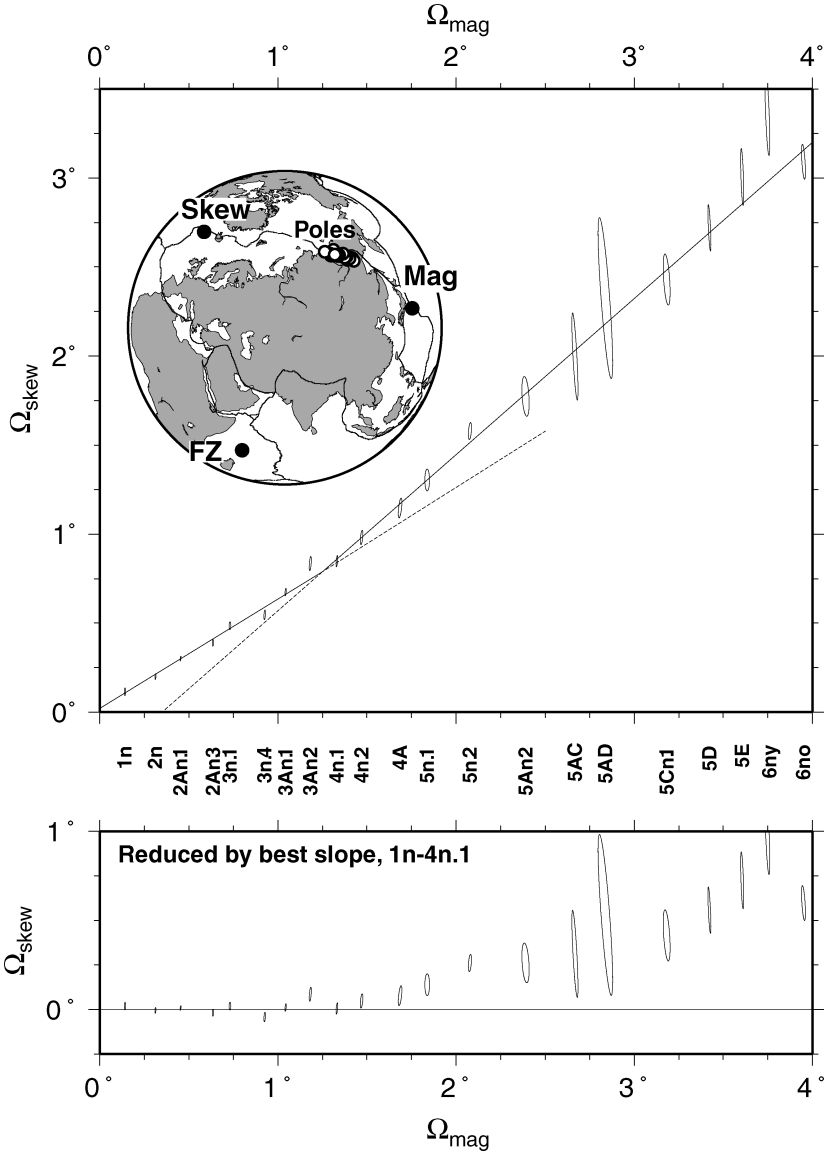

Figure 11. Orthogonal components of Eurasia–North America plate motion rotations (Table 3) and their 2-D, 1σ error ellipses projected onto the $\Omega_{\rm Skew}$, $\Omega_{\rm Mag}$ and $\Omega_{\rm FZ}$ axes indicated on the inset globe. The rotation components that are aligned with the $\Omega_{\rm Skew}$ and $\Omega_{\rm Mag}$ axes describe the opening gradient and pure opening components of motion along the plate boundary and increase linearly in time for a fixed pole and steady angular rotation rate. The dimensionless ratio of these two rotation components is insensitive to possible errors in reversal ages. Changes in the ratio of these two component angles, shown in the upper diagram, are thus robust indicators of a change in plate motion (Wilson 1993). The lower diagram shows the same angle pairs after removing the slope that best fits the angle pairs for Anomalies 1n–4n.1, thereby emphasizing the obvious change in motion at Anomaly 4n.1 (7.5 Ma).

we selected for one or more magnetic reversals. For example, the anomalously fast stage rate for the interval from 7.5 to 9.1 Ma and anomalously slow rate for the interval from 9.1 to 11.0 Ma (both shown by grey-shaded circles in Fig. 13a) share in common the plate motion rotation for Anomaly 4A (9.1 Ma). We suspect that either the estimated age for Anomaly 4A is slightly too young or that we systematically picked this reversal point several hundred metres too far from the spreading axis—either would cause the apparent stage rate to be too fast for the younger interval and too slow for the older interval.

In summary, the orthogonal rotation angles, stage poles and stage opening rates clearly define a transition in plate motion at 7.5–6.7 Ma (Anomaly 4n.1–3An.2). The transition was preceded and followed by long periods of steady motion, with any changes in seafloor spreading rates from 20 to 7.5 Ma smaller than 4 per cent ($\pm$1 mm yr^{-1}) and even smaller variations ($\pm$2 per cent) from 6.7 Ma to the present. The directions of motion that are predicted by the stage rotations (Fig. 11b) suggest that a several degree counter-clockwise rotation of the opening direction occurred at 7.5–6.5 Ma, consistent with the observed eastward migration of the finite plate motion poles (Fig. 12) and a $\sim$10° counter-clockwise rotation of the magnetic lineations that flank the Kolbeinsey Ridge north of Iceland (Fig. 14a).

4.6 Limits on the timing and steadiness of motion since 7.5 Ma

We used the plate motion rotations for times younger than 8 Ma to determine an upper limit for any recent changes in motion and

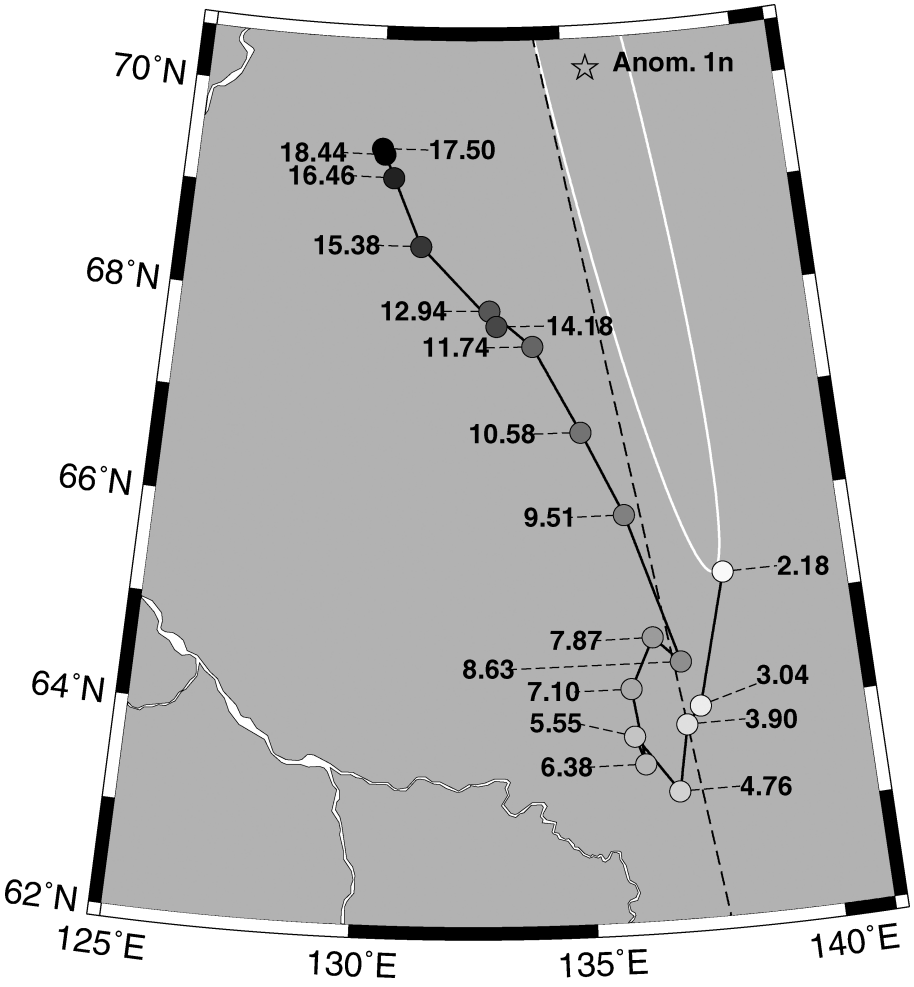

Figure 12. Anomaly 1n pole (Table 3) with standard error ellipse and time-progression of Eurasia–North America plate motion poles determined from running weighted averages of groups of four sequential poles (Table 3) and their uncertainties (Table 2). Labels correspond to the average age in million years of the reversals used to calculate a given average pole location. The youngest pole (2.18 Ma) averages over Anomalies 1n, 2n, 2An.1 and 2An.3 and the oldest pole (18.44 Ma) averages over Anomalies 5D, 5E, 6ny and 6no. Dashed line shows the great circle that connects the 3.9 Ma-average pole, which is located near the approximate centroid of poles younger than 7 Ma, to a point along the Reykjanes Ridge. All poles located along this great circle predict the same direction at that point. Circle shading is solely for visual clarity.

assess how far into the past, motion has remained steady. Steady motion between the Eurasia and North America plates implies a fixed pole of opening and constant rate of angular opening. We therefore searched systematically for the pole and angular rotation rate that best approximate the sequence of eight plate motion rotations for Anomalies 1n–3An.2 (Table 3). We define the least-squares difference χ^2 between a single plate motion rotation and trial rotation using $\chi^2 = \Delta\Omega\, \mathrm{W}^{-1} \Delta\Omega^T$, where W is the 3×3 covariance matrix of that best-fitting plate motion rotation, $\Delta\Omega$ is the 1×3 vector difference between the Cartesian components of the best-fitting and trial rotations and $\Delta\Omega^T$ is its transpose. The cumulative least-squares difference between the sequences of plate motion rotations for Anomalies 1n–3An.2 and a single trial pole and assumed rate of angular opening is therefore the sum of the χ^2 difference between each plate motion rotation and its corresponding trial rotation, in which the trial pole is fixed and the trial opening angle equals the assumed angular opening rate multiplied by the age of the corresponding plate motion rotation.

The pole and angular rotation rate that minimize χ^2 for Anomalies 1n to 3An.2 are 64.2°N, 137.2°E and 0.210° Myr^{-1}, with covariances of σ_{xx} =0.77, $\sigma_{xy} = -0.33$, $\sigma_{xz} = 1.54$, $\sigma_{yy} = 0.26$, $\sigma_{yz} = -0.97$ and $\sigma_{zz} = 4.06$, all in units of radians^2 Myr^{-2}. As is shown in Fig. 13a, all but one of the stage rates for the past 6.7 Myr agree with the seafloor spreading rate that is predicted from the constant-motion angular velocity vector to within 0.4 mm yr^{-1}. These small differences suggest that any change in motion since 6.7 Ma has been less than 2 per cent (0.4 mm yr^{-1}) of the full spreading rate. The stage directions are also consistent with constant motion within their several degree uncertainties (Fig. 13b).

We also tested models in which the present period of constant motion is assumed to have started at or before Anomaly 4n.1 (7.5 Ma). We find, however, that the cumulative χ^2 differences between the assumed constant motion models and their corresponding sequences of plate motion rotations increase rapidly, indicating that the plate motion rotations are inconsistent with the assumption that the pole and rate of angular opening remained constant over periods longer than the past 6.7 Myr. We therefore conclude that the present period of constant Eurasia–North America motion began no earlier than 6.7 Ma and that variations in the rate of motion during this period are unlikely to exceed 2 per cent at high confidence level.

Our preliminary estimates of best-fitting rotations for anomalies older than Anomaly 6no suggest that the apparently steady motion

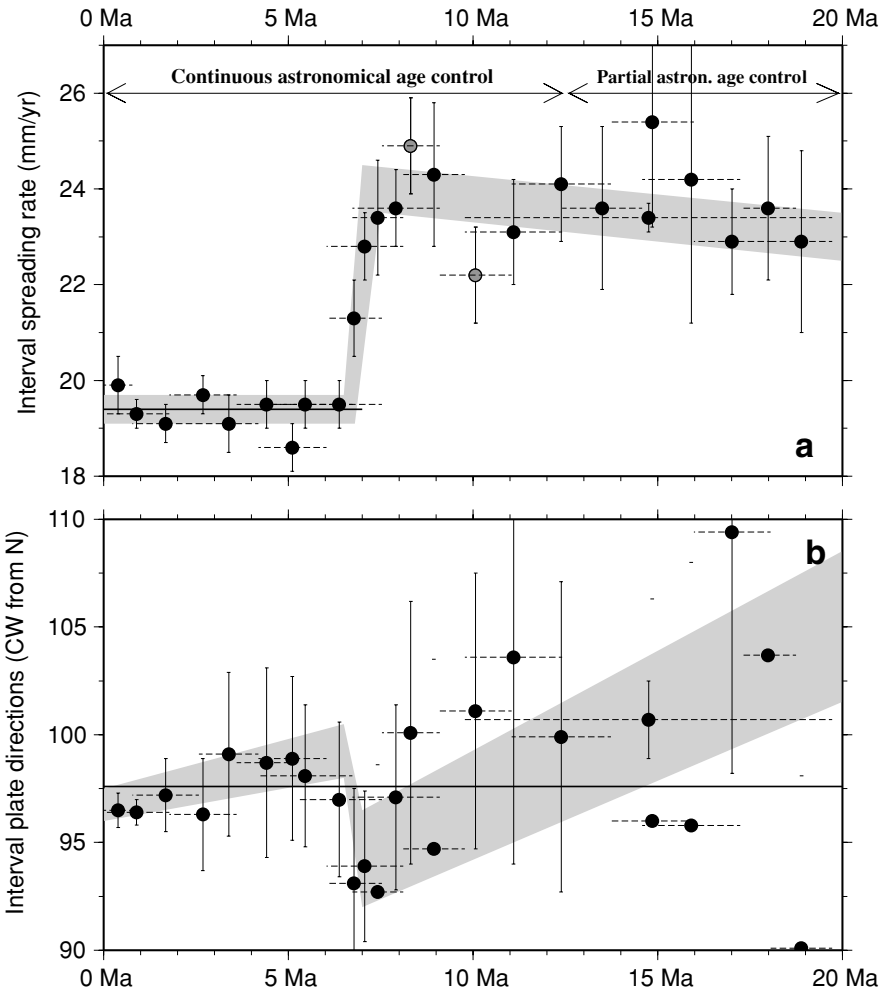

Figure 13. Interval seafloor spreading rates (a) and directions (b) since 20 Ma estimated from stage plate motion rotations. Velocities are predicted at 59.2°N, 29.4°W along the Reykjanes Ridge. The horizontal line from 0 to 7 Ma shows the opening rate predicted by a steady-motion model for the present back to the time of Anomaly 3An.2 (Section 4.6). Horizontal dashed lines specify the time interval spanned by a given stage rotation. All rates are corrected for outward displacement. Shaded stage rates have anticorrelated errors that are discussed in Section 4.5.3

from 20 to 7.5 Ma began before the time of Anomaly 6no. We therefore defer consideration of the duration and degree of steadiness of plate motion during this older period to a future paper.

5 DISCUSSION AND CONCLUSIONS

5.1 India–Somalia and Eurasia–North America motion changes

Fig. 15 illustrates the rates that are predicted by our new model for Eurasia–North America motion relative to those predicted by an equally detailed model of India–Somalia motion since 20 Ma (Merkouriev & DeMets 2006). Although the Indian and Eurasian plates share a wide convergent boundary in southern Asia, their seafloor spreading kinematic records show no obvious correlation, as might have been expected if the motions of these two plates were tightly coupled across their convergent boundary. For example, the 25–30 per cent slowdown in India–Somalia seafloor spreading rates from 20 to 10 Ma that ceased at $\sim 9 \pm 1$ Ma preceded the change in Eurasia–North America motion at 7.5–6.7 Ma by several million years. Similarly, the well-defined change in Eurasia–North America motion at 7.5–6.7 Ma had no discernible effect on India–Somalia motion at that time. The motions of the Indian plate relative to Somalia and Eurasia plate relative to North America thus appear to be decoupled despite the wide shared boundary between the Indian and Eurasian plates.

5.2 Cause of Kolbeinsey ridge reorganization

Appelgate (1997) hypothesizes that the $\sim 5^\circ$ counter-clockwise rotation of the Kolbeinsey ridge axis during Anomaly 3A and corresponding formation of the Spar axial offset was either a response to a previously undetected change in plate motion during Anomaly 3A or a more localized response to increased magmatic vigour north of Iceland. Our kinematic analysis clearly indicates that Eurasia–North America motion changed at 7.5–6.7 Ma and therefore indicates that the changes in the axial geometry of the Kolbeinsey ridge during Anomaly 3A were a response to that change in plate motion. The magnetic lineations at other locations along the plate boundary show no evidence for a similar counter-clockwise rotation in their azimuths at 7.5–6.7 Ma (Figs 14a–d), indicating that the reconfiguration

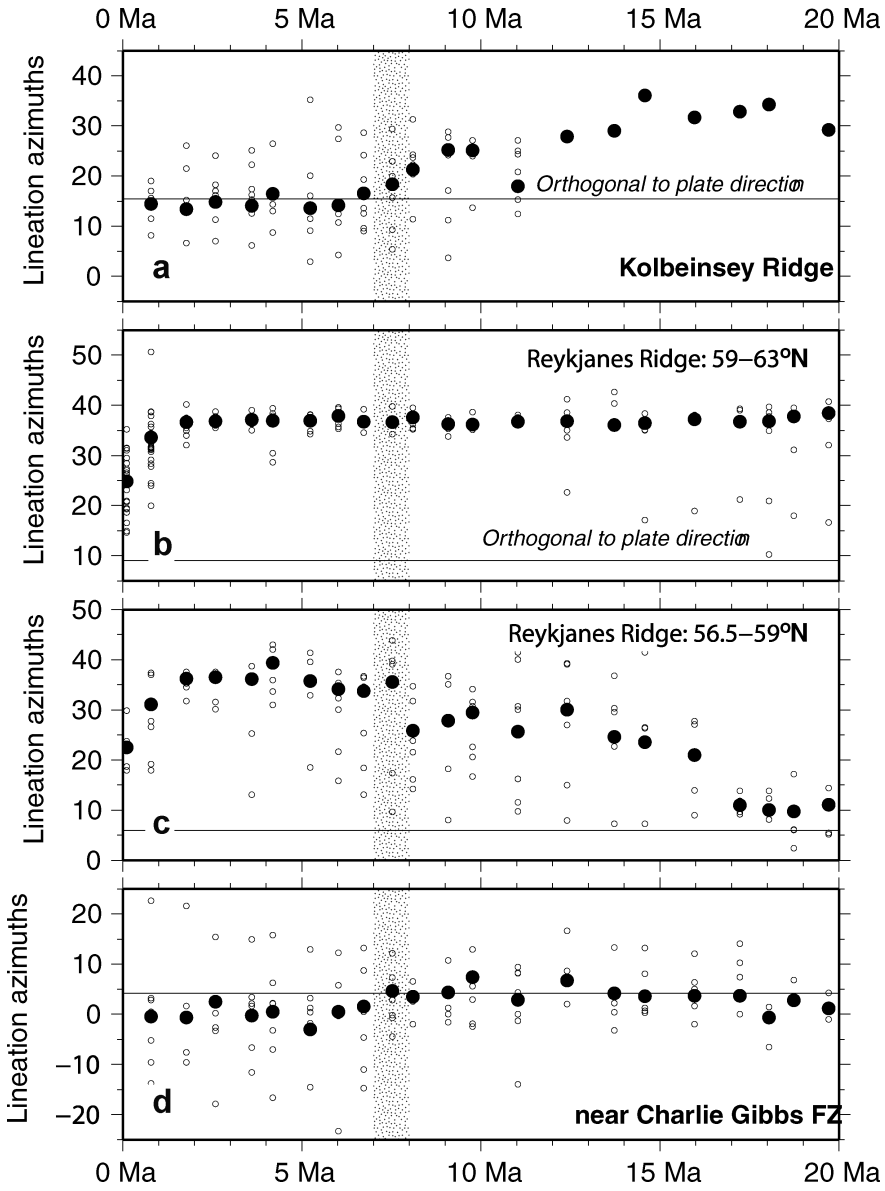

Figure 14. Time evolution of reconstructed magnetic lineation azimuths along Kolbeinsey and Reykjanes ridges and near the Charlie Gibbs fracture zone. Horizontal lines show directions orthogonal to the Eurasia–North America plate directions that are predicted for each area by the stationary pole model described in Section 4.6. Open circles are best-fitting azimuths for reconstructed magnetic lineations shown in Figs 8 and 9. Solid circles show mean lineation directions. Orientations of axial volcanic rises that define the present axis of the Reykjanes Ridge (b) are shown with an age of 0 Ma. Stippled areas indicate time when pole location changed.

of the Kolbeinsey Ridge axis was a localized response to the change in plate motion.

5.3 Deformation in northeastern Asia

Following the lead of previous authors (Cook *et al.* 1986; Riegel *et al.* 1993; Imaev *et al.* 2000; Gaina *et al.* 2002), we discuss the implications of our new kinematic model for the evolution of deformation within areas of northeastern Asia that are affected by Eurasia–North America motion. Cook *et al.* (1986) estimate a present-day Eurasia–North America rotation pole of 71.2°N, 132.0°E from the slip vectors of earthquakes in northeastern Asia and argue that the body of evidence available to them, consisting of their newly-derived pole location, pole locations for older times and structural observations were collectively consistent with a southward shift of the Eurasia–North America pole sometime after ∼10 Ma. They postulate that this southward pole shift would have induced a tensional stress regime in northeastern Asia that caused the Okhotsk plate to separate from North America, and further suggest that their postulated reconfiguration of regional block boundaries and creation of the Okhotsk plate permitted the Eurasia–North America pole to migrate back to its location near 71°N sometime after 3 Ma.

Our results confirm that the stage pole migrated southward after 10 Ma, as postulated by Cook *et al.*, but that the shift in the pole location was several million years earlier than proposed by Cook *et al.* More precisely, the stage pole that describes motion from 19.7 to 7.5 Ma (Fig. 16c), migrated approximately 650 km south to a new location in northeastern Asia at 7.5–6.7 Ma (Fig. 16b). This shift in the pole location altered the compressional stress regime that

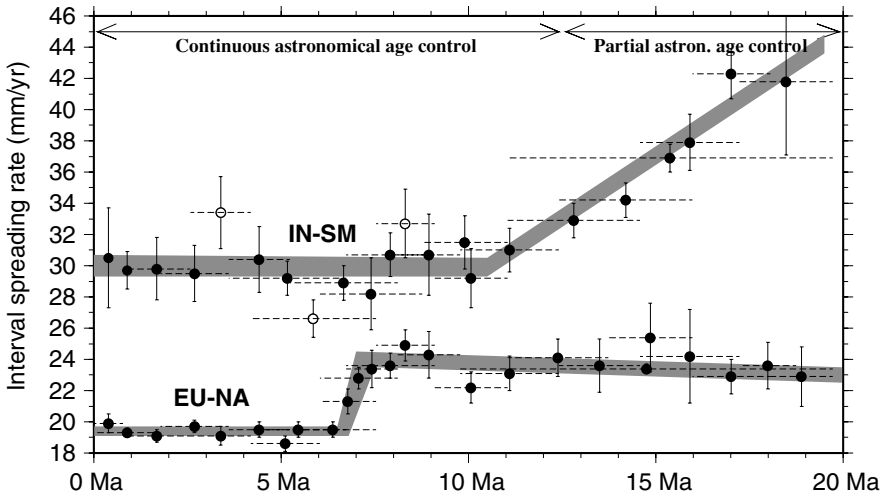

Figure 15. Comparison of India–Somalia (IN-SM) interval seafloor spreading rates from Merkouriev & DeMets (2006) and Eurasia–North America (EU-NA) interval rates. All of the rates employ identical, astronomically-tuned magnetic reversal ages (Lourens *et al.* 2004). Open circles designate rates that are subject to systematic bias due to difficulties in determining the precise reversal location for Anomalies 3n.1 and 4n.1. Eurasia–North America interval rates are from Fig. 13. All rates are corrected for the effect of outward displacement. Interval rates for times older than Anomaly 2 are largely unaffected by this correction due to differencing of the finite rotations to determine stage rotations. Horizontal dashed lines specify the time interval spanned by each rate.

prevailed before 7.5 Ma in large areas of northeastern Asia south of the pole to an extensional stress regime after 6.7 Ma.

Contrary to Cook *et al.*'s estimate of 71.2°N, 132.0°E for the present-day pole location, we find no evidence that the pole shifted northward back to a location close to 70°N over the past few million years. Our results instead indicate that the pole remained near 64°N until at least 1.78 Ma (Anomaly 2n) and more likely to the present. Seismic observations independently support this interpretation (Fig. 16). Left-lateral strike-slip focal mechanisms of earthquakes that occur along N–NNW trending faults in the Cherskii mountain range (Imaev *et al.* 2000) are consistent with both the sense and direction of motion that are predicted by our 6.7–0 Ma pole (Fig. 16a). Over a larger area, the tensional axes of earthquakes from the seismically active zones, which appear to separate the Eurasian and North American plates, are much better aligned with small circles around our 6.7–0 Ma pole (Fig. 16b), which predict principal directions of extension, than they are with small circles around a pole at 70°N (Fig. 16c). Although none of these unambiguously demonstrate that the present pole is located at 64°N, a model that postulates the existence of a relatively recent dramatic northward shift in the pole location appears to be more complex than is warranted by the available data.

5.4 Comparison with GPS estimates

The evidence described above for steady motion since 6.7 Ma suggests that GPS measurements at sites on the Eurasian and North American plates should yield short-term plate motion that agrees with our estimate of the long-term motion, barring any change in motion since 0.78 Ma. We compared GPS-based angular velocity vectors for Eurasia–North American plate motion from recent studies (Altamimi *et al.* 2002; Sella *et al.* 2002; Calais *et al.* 2003; Steblov *et al.* 2003; Altamimi *et al.* 2007) with the 6.7–0 Ma angular velocity vector to test our steady-motion hypothesis.

Fig. 17 shows GPS-derived Eurasia–North America pole locations from the above studies relative to the 6.7–0 Ma and Anomaly 1n pole locations. All five GPS poles are located north of the long-term pole and predict motion that either contradicts seismologic constraints or fits the seismic data more poorly than does the 6.7–0 Ma model. For example, the most recently published pole (Altamimi *et al.* 2007) predicts that convergence occurs at all locations along the plate boundary south of 77°N. This contradicts clear evidence for extension south of 77°N, including normal-faulting earthquake focal mechanisms (Fig. 16) and high heat flow and hydrothermal fauna in the Laptev Sea, which are consistent with active opening of the seismically active grabens (Drachev *et al.* 2003). Curiously, although the recently estimated GPS pole from Altamimi *et al.* (2007) is based on a large number of GPS stations with long coordinate time-series and uses the most recent realization of the international geodetic reference frame ITRF2005, it fits the seismic constraints more poorly than does an older pole that is based on fewer station velocities with shorter coordinate time-series and the older ITRF2000 geodetic reference frame (Altamimi *et al.* 2002).

The northward bias of all published GPS pole locations with respect to the long-term pole location may be evidence for either a northward shift of the pole of rotation since 0.78 Ma or, as we suspect, a systematic bias in most or all GPS estimates. Steblov *et al.* (2003) demonstrate that GPS estimates of Eurasia plate motion that rely principally on European GPS stations and are tied to present or past realizations of the International Geodetic Reference Frame (ITRF) yield Eurasia–North America poles that lie too far north. They further show that the GPS-derived pole location shifts south toward the 3.16 Ma-average NUVEL-1A Eurasia–North America pole location (DeMets *et al.* 1994) (and our 6.7 Ma to present pole location) if they relax the constraint that ties GPS station velocities to ITRF and employ GPS velocities with more even geographic coverage of the Eurasian plate, including stations in northeastern Asia that are close to the present pole.

The two GPS poles closest to our 6.7–0 Ma pole (Fig. 17), those of Sella *et al.* (2002) and Steblov *et al.* (2003), predict respective opening rates of 21.5 ± 0.2 and 20.2 ± 0.5 mm yr^{-1} along the Reykjanes Ridge flow line. The former rate is significantly faster than the 19.4 ± 0.25 mm yr^{-1} opening rate predicted by our 6.7–0 Ma model. The latter GPS-based opening rate is however

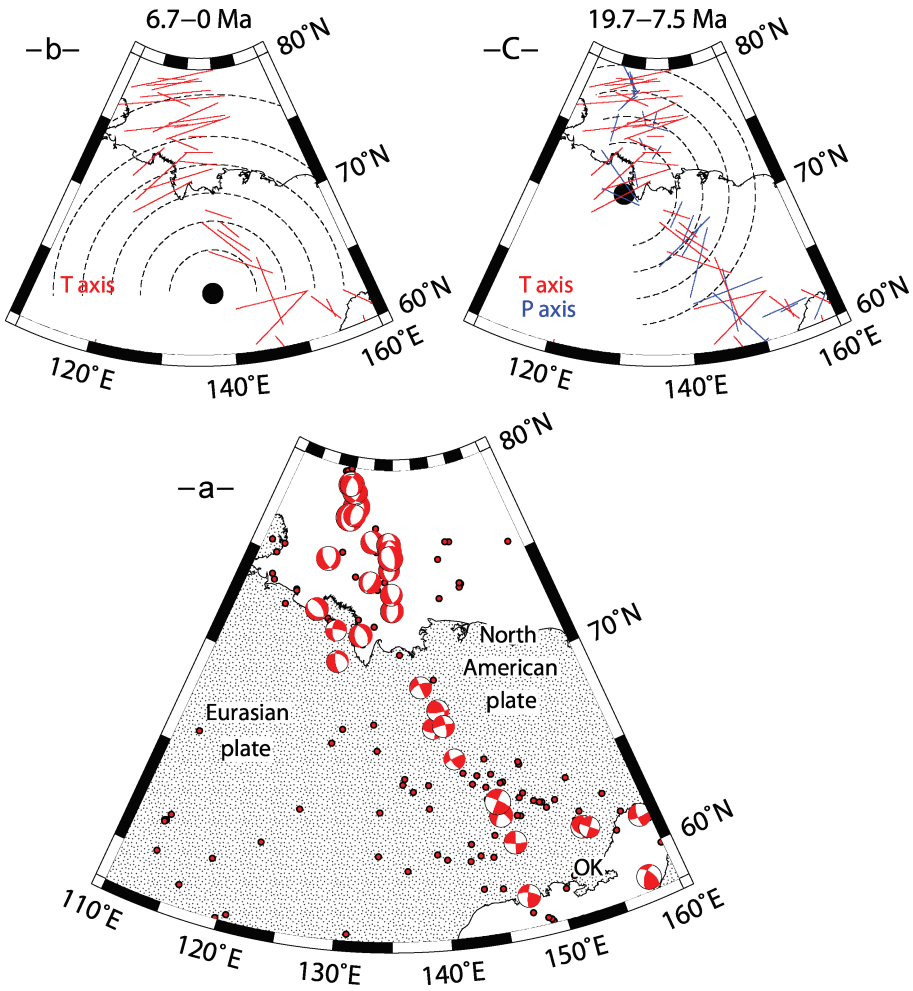

Figure 16. A - Seismicity and earthquake focal mechanisms of northeastern Asia. Earthquakes include events of all magnitudes above depths of 60 km from 1963 to 2007. Focal mechanisms are compiled from Harvard centroid moment tensor solutions for 1977–2007 and Cook *et al.* (1986) and Riegel *et al.* (1993) for times earlier than 1977. 'OK' designates Okhotsk plate. Panels b and c show, respectively, tensional (red) and pressure (blue) axes of focal mechanisms with their lengths scaled to earthquake magnitudes and axis plunges. Small circles depict trajectories around the 6.7–0 Ma constant-motion pole of 64.2°N, 137.2°E (Panel b) and the 19.7–7.5 Ma stage pole at 71.0°N, 127.9°E (Panel c)

consistent with our long-term estimate within their combined uncertainties.

Based on the widely varying locations of published GPS poles (Fig. 17) and differences of several mm yr^{-1} between the opening rates that are predicted by the same GPS solutions, we suspect that the formal uncertainties for Eurasia–North America motion that are estimated by the authors of published GPS models significantly understate their true uncertainties, most likely because the GPS solutions fail to account for significant sources of systematic error. We conclude that GPS estimates are still too uncertain for a strong test of our hypothesis that Eurasia–North America motion has remained constant since 6.7 Ma.

5.5 Plate dynamics

Our results clearly suggest that Eurasia–North America motion since 20 Ma is well described by a model that consists of two long periods of steady motion during which any variations in motion were smaller than the ±0.5–1 mm yr^{-1} resolution of our analysis. The abrupt change in motion at 7.5–6.5 Ma is perhaps the most interesting new result to emerge from this work. We suspect that geodynamic modelling could be used to study and rule out broad classes of possible explanations for the forces that might have induced the observed change. For example, given the broad expanse of convergent plate boundaries at Eurasia's southern edge, a change in the configuration of faults or the forces that were acting along one of these convergent boundaries might have caused the change in Eurasia–North America motion. Alternatively, a southeastward propagation of the Eurasia–North America plate boundary through northeastern Asia to the Pacific plate, as proposed by Cook *et al.* (1986), may have altered the effective ratio of convergent and divergent areas of the plate boundary and hence could have effected an abrupt change in the net torque that was acting on these two plates.

ACKNOWLEDGMENTS

We thank Carmen Gaina for supplying us with her magnetic anomaly picks for consistency checks. This work was supported by grant 06-05-64297 from the Russian Foundation for Basic Research and grant INT-0244894 from the U.S. National Science Foundation. Figures were drafted using Generic Mapping Tools software (Wessel & Smith 1991).

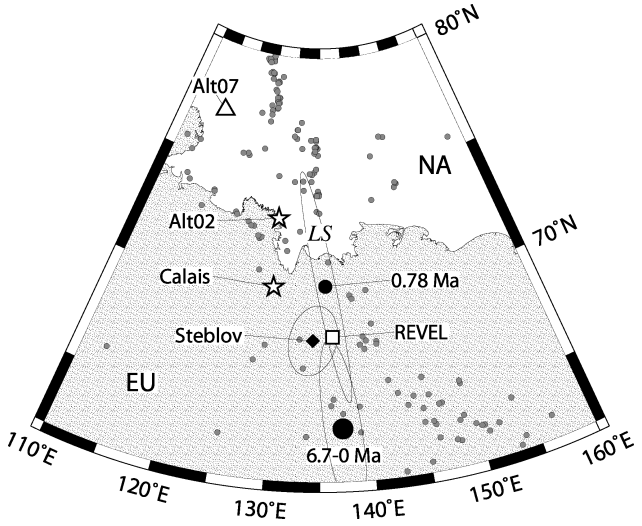

Figure 17. Candidate rotation poles for present-day Eurasia–North America plate motion. Poles shown by filled circles are from this study. All ellipses are 2-D, 1σ confidence regions. Poles shown by the square, star, and triangle, respectively, use geodetic reference frames of ITRF1997, ITRF2000 and ITRF2005. Pole sources are REVEL – Sella *et al.* (2002); Alt02 – Altamimi *et al.* (2002); Calais – Calais *et al.* (2003); Steblov – Steblov *et al.* (2003); Alt07 – Altamimi *et al.* (2007); LS – Laptev Sea.

REFERENCES

Altamimi, Z., Sillard, P. & Boucher, C., 2002. ITRF2000: a new release of the International Terrestrial Reference Frame for earth science applications, *J. geophys. Res.,* **107,** 2214, doi:10.1029/2001JB000561.

Altamimi, Z., Collilieux, X., Legrand, J., Garayt, B. & Boucher, C., 2007. ITRF2005: a new release of the International Terrestrial Reference frame based on time-series of station positions and earth orientation parameters, *J. geophys. Res.,* **112,** B09401, doi:10.1029/2007JB004949.

Appelgate, B., 1997. Modes of axial reorganization on a slow-spreading ridge: the structural evolution of the Kolbeinsey Ridge since 10 Ma, *Geology,* **25,** 431–434.

Calais, E., DeMets, C. & Nocquet, J.-M., 2003. Evidence for a post-3.16 Ma change in Nubia–Eurasia–North America plate motions, *Earth planet. Sci. Lett.,* **216,** 81–92.

Chang, T., 1988. Estimating the relative rotation of two tectonic plates from boundary crossings, *J. Am. Stat. Assoc.,* **83,** 1178–1183.

Cook, D.B., Fujita, K. & McMullen, C.A., 1986. Present-day interactions in northeast Asia: North American, Eurasian, and Okhotsk plates, *J. Geodyn.,* **6,** 33–51.

DeMets, C. & Wilson, D.S., 2008. Toward a minimum change model for recent plate motions: calibrating seafloor spreading rates for outward displacement, *Geophys. J. Int.,* review.

DeMets, C., Gordon, R.G., Argus, D.F. & Stein, S., 1994. Effect of recent revisions to the geomagnetic reversal timescale on estimates of current plate motions, *Geophys. Res. Lett.,* **21,** 2191–2194.

Drachev, S.S., Kaul, N. & Beliaev, V.N., 2003. Eurasia spreading basin to Laptev Shelf transition: structural pattern and heat flow, *Geophys. J. Int.,* **152,** 688–698.

Fisher, N.I., Lewis, T. & Embleton, B.J. J., 1993. *Statistical Analysis of Spherical Data*, Cambridge University Press, Cambridge, 329 pp.

Gaina, C., Roest, W.R. & Muller, R.D., 2002. Late Cretaceous-Cenozoic deformation of northeast Asia, *Earth planet. Sci. Lett.,* **197,** 273–286.

Gente, P., Dyment, J., Maia, M. & Goslin, J., 2003. Interaction between the Mid-Atlantic Ridge and the Azores hot spot during the last 85 Myr: emplacement and rifting of the hot spot-derived plateaus, *Geochem. Geophys. Geosys.,* **4**(10), 8514, doi:10.1029/2003GC000527.

Glebovsky, V.Y., Kaminsky, V.D., Minakov, A.N., Merkuriev, S.A., Childers, V.A. & Brozena, J.M., 2006. Formation of the Eurasia Basin in the Arctic Ocean as inferred from geohistorical analysis of the anomalous magnetic field, *Geotectonics,* **40,** 263–281.

Goslin, J.H. & Triatnord Scientific Party, 1999. Extent of Azores plume influence on the Mid-Atlantic Ridge north of the hotspot, *Geology,* **27,** 991–994.

Hellinger, S.J., 1979. The statistics of finite rotations in plate tectonics, unpublished *PhD thesis*, Massachusetts Institute of Technology, 172 pp.

Imaev, V.S., Imaeva, L.P., Koz'min, B.M., Gunbina, L.V., Mackey, K.G. & Fjuita, K., 2000. Seismicity and present-day boundaries of plates and blocks in northeast Asia, *Geotectonics,* **34,** 294–301.

Kogan, M.G. *et al.*, 2000. Geodetic constraints on the rigidity and relative motion of Eurasia and North America, *Geophys. Res. Lett.,* **27,** 2041–2044.

Lawver, L.A., Muller, R.D., Srivastava, S.P. & Roest, W., 1990. The opening of the Arctic Ocean, in *Geologic History of the Polar Oceans: Arctic Versus Antarctic*, pp. 29–62, eds Bleil, U. & Thiede, E.J., NATO Symposium, Bremen, October, 1988.

Lourens, L., Hilgen, F.J., Laskar, J., Shackleton, N.J. & Wilson, D., 2004. The Neogene Period, in *A Geologic Time Scale 2004*, pp. 409–440, eds Gradstein, F., Ogg, J. & Smith, A., Cambridge University Press, London.

Macnab, R., Verhoef, J., Roest, W. & Arkani-Hamed, J., 1995. New database documents the magnetic character of the Arctic and North Atlantic, *EOS, Trans. Am. geophys. Un.* **76,** 449, 458.

Merkouriev, S. & DeMets, C., 2006. Constraints on Indian plate motion since 20 Ma from dense Russian magnetic data: implications for Indian Plate dynamics, *Geochem. Geophys. Geosys.,* **7,** Q02002, doi:10.1029/2005GC001079.

Moore, D.G., Curray, J.R., Raitt, R.W. & Emmel, F.J., 1974. Stratigraphic-seismic section correlations and implications to Bengal Fan history, *Initial Rep. Deep Sea Drill. Proj.,* **22,** 403–412.

Paul, J. *et al.*, 2001. The motion and active deformation of India, *Geophys. Res. Lett.,* **28,** 647–651.

Pitman, W.C. & Talwani, M., 1972. Sea floor spreading in the North Atlantic, *Bull. geol. Soc. Am.,* **83,** 619–646.

Riegel, S.A., Fujita, K., Koz'min, B.M., Imaev, V.S. & Cook, D.B., 1993. Extrusion tectonics of the Okhotsk plate, northeast Asia, *Geophys. Res. Lett.,* **20,** 607–610.

Rowley, D.B. & Lottes, A.L., 1988. Plate-kinematic reconstructions of the North Atlantic and Arctic: late Jurassic to present, *Tectonophysics,* **155,** 73–120.

Royer, J.-Y. & Chang, T., 1991. Evidence for relative motions between the Indian and Australian plates during the last 20 Myr from plate tectonic reconstructions: implications for the deformation of the Indo-Australian plate, *J. geophys. Res.,* **96,** 11 779–11 802.

Sandwell, D.T. & Smith, W.H.F., 1997. Marine gravity anomaly from Geosat and ERS 1 altimetry, *J. geophys. Res.,* **102,** 10 039–10 054.

Searle, R.C., Keeton, J.A., Owens, R.B., White, R.S., Mecklenburgh, R., Parson, B. & Lee, S.M., 1998. The Reykjanes Ridge: structure and tectonics of a hot-spot-influenced, slow-spreading ridge, from multibeam bathymetry, gravity, and magnetic investigations, *Earth planet. Sci. Lett.,* **160,** 463–478.

Sella, G.F., Dixon, T.H. & Mao, A., 2002. REVEL: a model for recent plate velocities from space geodesy, *J. geophys. Res.,* **107**(B4), doi:10.1029/2000JB000033.

Sempere, J-C., Macdonald, K.C. & Miller, S.P., 1987. Detailed study of the Brunhes/Matuyama reversal boundary on the East Pacific Rise at 19°30′S: implications for crustal emplacement processes at an ultra fast spreading center, *Mar. geophys. Res.,* **9,** 1–23.

Sempere, J.-C., Kristjansson, L., Schouten, H., Heirtzler, J.R. & Johnson, G.L., 1990. A detailed magnetic study of the Reykjanes Ridge between 63°00′N and 63°40′N, *Mar. geophys. Res.,* **12,** 215–234.

Srivastava, S.P. & Tapscott, C.R., 1986. Plate kinematics of the North Atlantic Plate, in *The Western North Atlantic Region*, The Geology of North

America M, eds Vogt, P.R. & Tucholke, B.E., pp. 379–405, Geol. Soc. Am., Boulder.

Steblov, G.M., Kogan, M.G., King, R.W., Scholz, C.H., Burgmann, R. & Frolov, D.I., 2003. Imprint of the North American plate in Siberia revealed by GPS, *Geophys. Res. Lett.,* **30**(18), 1924, doi:10.1029/2003GL017805.

Stock, J.M. & Molnar, P., 1983. Some geometrical aspects of uncertainties in combined plate reconstructions, *Geology,* **11,** 697–701.

Verhoef, J., Roest, W., Macnab, R., Arkani-Hamed, J. & Members of the Project Team, 1996. Magnetic anomalies of the Arctic and North Atlantic Oceans and adjacent land areas, GSC Open File 3125, parts a and b (CD-ROM and project report), Geological Survey of Canada, Dartmouth, Nova Scotia, 225 pp.

Vogt, P.R., Johnson, G.L. & Kristjansson, L., 1980. Morphology and magnetic anomalies north of Iceland, *J. Geol.,* **47,** 67–80.

Wessel, P. & Smith, W.H.F., 1991. Free software helps map and display data, *EOS, Trans. Am. geophys. Un.,* **72,** 441–446.

Wilson, D.S., 1993. Confidence intervals for motion and deformation of the Juan de Fuca plate, *J. geophys. Res.* **98,** 16 053–16 071.

SUPPLEMENTARY MATERIAL

The following supplementary material is available for this article:

Fig. S1. Reykjanes Ridge magnetic data. Oblique Mercator projection (PS format).

Fig. S2. Magnetic anomaly data along the Kolbeinsey Ridge (upper panel) and near the Charlie Gibbs fracture zone (lower panel). Mercator projection. Magnetic data in (A) are from a low-altitude aeromagnetic survey done by the U.S. Naval Oceanographic Office (Vogt *et al.* 1980) and data in (B) are from Russian ship survey AK89 (Fig. 2) (PS format).

Fig. S3. Magnetic anomaly data north of the Azores triple junction. Mercator projection (PS format).

This material is available as part of the online article from: http://www.blackwell-synergy.com/doi/abs/10.1111/j.1365-246X.2008.03761.x
(This link will take you to article abstract).

Please note: Blackwell Publishing are not responsible for the content or functionality of any supplementary materials supplied by authors. Any queries (other than missing material) should be directed to the corresponding author for the article.